Temporal and spatial trends of Late Cretaceous-early Tertiary underplating of Pelona and related schist beneath southern California and southwestern Arizona

M. Grove
*Department of Earth and Space Sciences, University of California, 595 Charles Young Drive E,
Los Angeles, California 90095-1567, USA*

Carl E. Jacobson
Department of Geological and Atmospheric Sciences, Iowa State University, Ames, Iowa 50011-3212, USA

Andrew P. Barth
Department of Geology, Indiana University–Purdue University, Indianapolis, Indiana 46202-5132, USA

Ana Vucic
Department of Geological and Atmospheric Sciences, Iowa State University, Ames, Iowa 50011-3212, USA

ABSTRACT

The Pelona, Orocopia, and Rand Schists and the schists of Portal Ridge and Sierra de Salinas constitute a high–pressure-temperature terrane that was accreted beneath North American basement in Late Cretaceous–earliest Tertiary time. The schists crop out in a belt extending from the southern Coast Ranges through the Mojave Desert, central Transverse Ranges, southeastern California, and southwestern Arizona. Ion microprobe U-Pb results from 850 detrital zircons from 40 metagraywackes demonstrates a Late Cretaceous to earliest Tertiary depositional age for the sedimentary part of the schist's protolith. About 40% of the ^{206}Pb/^{238}U spot ages are Late Cretaceous. The youngest detrital zircon ages and post-metamorphic mica ^{40}Ar/^{39}Ar cooling ages bracket when the schist's graywacke protolith was eroded from its source region, deposited, underthrust, accreted, and metamorphosed. This interval averages 13 ± 10 m.y. but locally is too short (<~3 m.y.) to be resolved with our methods. The timing of accretion decreases systematically (in palinspastically restored coordinates) from about 91 ± 1 Ma in the southwesternmost Sierra Nevada (San Emigdio Mountains) to 48 ± 5 Ma in southwest Arizona (Neversweat Ridge). Our results indicate two distinct source regions: (1) The Rand Schist and schists of Portal Ridge and Sierra de Salinas were derived from material eroded from Early to early Late Cretaceous basement (like the Sierra Nevada batholith); and (2) The Orocopia Schist was derived from a heterogeneous assemblage of Proterozoic, Triassic, Jurassic, and latest Cretaceous to earliest Tertiary crystalline rocks (such as basement in the Mojave/Transverse Ranges/southwest Arizona/northern Sonora). The Pelona Schist is transitional between the two.

Keywords: Pelona Schist, Orocopia Schist, Rand Schist, detrital mineral, zircon, U-Pb.

INTRODUCTION

The dramatic Laramide craton-ward shift of arc magmatism and contractional deformation was arguably the most important development in the Late Cretaceous–early Tertiary evolution of western North America (Coney and Reynolds, 1977; Dickinson and Snyder, 1978; Bird, 1988). In southern California and adjacent areas, the Pelona, Orocopia, and Rand Schists and the schists of Portal Ridge and Sierra de Salinas have been widely considered to be a product of this event (e.g., Burchfiel and Davis, 1981; Crowell, 1981; Hamilton, 1987, 1988). Referred to collectively in this paper as the "schists," these rocks comprise a distinctive eugeoclinal assemblage that was metamorphosed from epidote-blueschist to oligoclase–amphibolite facies at pressures of ~700–1000 MPa (Fig. 1; Ehlig, 1958, 1968, 1981; Crowell, 1968, 1981; Yeats, 1968; Haxel and Dillon, 1978; Jacobson, 1983a, 1995; Graham and Powell, 1984; Jacobson et al., 1988, 1996, 2002a; Dillon et al., 1990; Malin et al., 1995; Wood and Saleeby, 1997; Haxel et al., 2002). The schists are juxtaposed beneath an upper plate of Precambrian to Mesozoic igneous and metamorphic rocks, with essentially no evidence of intervening lithospheric mantle. They underlie a series of low-angle faults known as the Vincent–Chocolate Mountains fault system. A few of these faults may be remnants of the thrust(s) beneath which the schists underwent prograde metamorphism (Ehlig, 1981; Jacobson, 1983b, 1997), but most are retrograde or postmetamorphic features responsible for exhumation of the schists (Haxel et al., 1985, 2002; Silver and Nourse, 1986; Jacobson et al., 1988, 1996, 2002a; Malin et al., 1995; Wood and Saleeby, 1997; Yin, 2002).

Many Cordilleran geologists have viewed the schists as accretionary rocks analogous to the Franciscan Complex that were underthrust beneath southern California during low-angle, northeast-dipping subduction of the Farallon plate (Fig. 2A; "subduction" model; Crowell, 1968, 1981; Yeats, 1968; Burchfiel and Davis, 1981; Hamilton, 1987, 1988; Jacobson et al., 1996; Malin et al., 1995; Wood and Saleeby, 1997; Yin, 2002). In fact, a correlation between the Pelona Schist and the Franciscan Complex was first suggested on the basis of lithologic and petrologic similarities even before the advent of plate tectonic theory (Ehlig, 1958; Woodford, 1960). The subduction model requires that lowermost North American continental crust and underlying mantle lithosphere were tectonically eroded by shallow subduction of the Farallon slab prior to accretion of the schist.

Hall (1991), Barth and Schneiderman (1996), and Saleeby (1997) have presented an alternative hypothesis in which the schist is considered to be a correlative of the Great Valley Group that was underthrust beneath a northeast-dipping fault between arc and forearc (Fig. 2B; "forearc" model). As with the subduction model, the forearc interpretation calls upon low-angle subduction of the northeast-dipping Farallon plate during the Laramide orogeny as the ultimate driving force for emplacement of the schists. However, in the forearc model, the Vincent–Chocolate Mountains thrust is viewed as a structure *within* the overriding North American plate rather than comprising the

plate boundary. As such, it does not require wholesale removal of lithospheric mantle, consistent with the modern example of the Andes, where South American mantle lithosphere is only partly thinned above the flat Nazca plate (Smalley and Isacks, 1987; Isacks, 1988; Allmendinger et al., 1990).

Additional models for the origin of the schist do not attempt to relate it to Laramide deformation. These models were motivated by early structural studies that indicated top-to-northeast sense of shear along the Chocolate Mountains fault in southeastern California (Dillon, 1976; Haxel, 1977). While it is now generally accepted that this shear sense was imparted during exhumation of the schist (Simpson, 1990; Jacobson et al., 1996, 2002a; Oyarzabal et al., 1997; Haxel et al., 2002; Yin, 2002), two distinct models involving southwest-dipping thrusts were born out of the early work. One of these that held that the schists formed during collision between North America and an exotic microcontinent (Fig. 2C; "Collision" model; Haxel and Dillon, 1978; Vedder et al., 1983) quickly lost favor as it became apparent that the proposed allochthon exhibited clear North American affinities (Haxel et al., 1985; Barth, 1990; Tosdal, 1990; Bender et al., 1993). A second interpretation has persisted, however. It postulates that the schist's protolith was deposited during rifting in a backarc setting within the North American craton (Haxel and Dillon, 1978; Ehlig, 1981). Haxel and Tosdal (1986) went a step further in suggesting that the backarc basin formed during activity along the proposed Mojave–Sonora Megashear of Silver and Anderson (1974). Overall, the backarc model has proven difficult to reconcile with the geology of southern California and western Arizona in that independent evidence for either the opening of the necessary rift basin or the suture that would have formed when it was closed is lacking (Burchfiel and Davis, 1981; Crowell, 1981; Hamilton, 1987, 1988). Very recently, Haxel et al. (2002) dealt with the apparent absence of a suture by proposing that all remnants of the closed backarc basin and the suture itself were restricted to a tectonic window beneath counterposed thrust faults (Fig. 2D). This model is similar to one that is used to explain concealment of the suture between India and Asia in southern Tibet (Yin et al., 1994; Harrison et al., 2000).

A major consideration in evaluating the validity of the models described above is provided by reports of pre-Late Cretaceous U-Pb ages from igneous bodies inferred to crosscut the schist (Mukasa et al., 1984; James, 1986; James and Mattinson, 1988). In particular, Mukasa et al.'s (1984) determination of a 163 Ma crystallization age for a mafic metadiorite within Orocopia Schist of the Chocolate Mountains has been widely cited as indicating a pre–Late Jurassic depositional age for the schist's protolith (Mattinson and James, 1985; Drobeck et al., 1986; Reynolds, 1988; Dillon et al., 1990; Grubensky and Bagby, 1990; Simpson, 1990; Powell, 1993; Richard, 1993; Sherrod and Hughes, 1993; Barth and Schneiderman, 1996; Miller et al., 1996; Robinson and Frost, 1996; Richard et al., 2000). An entirely pre–Late Jurassic depositional age for the schist's protolith would strongly disfavor the subduction and forearc models since they identify either the Late Cretaceous subduction trench or forearc basin as the source of graywacke sediment that was underthrust during Laramide shal-
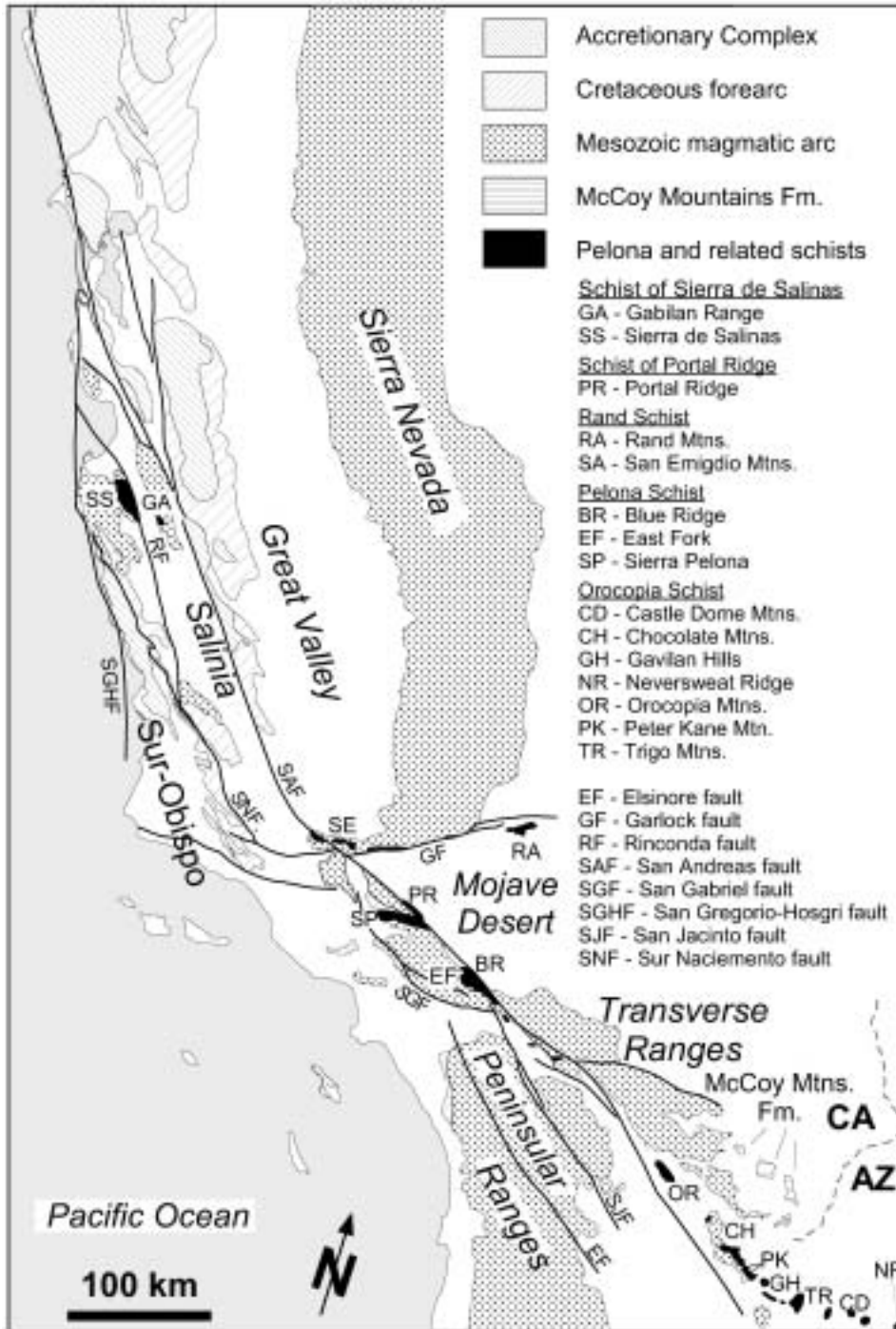
Figure 1. Schematic geologic map of central and southern California and southwesternmost Arizona showing distribution of Pelona and related schists. Note that simple geometry of medial Cretaceous Sierran arc, Great Valley forearc basin, and subduction complex in central California is highly disrupted within southern Coast Ranges and Transverse Ranges of southern California; AZ—Arizona, CA—California. Simplified from Jennings (1977).

low subduction. Alternatively, Haxel and Tosdal (1986) pointed out that the backarc model could agree well with a pre–Late Jurassic depositional age if the rift basin formed in response to activity along the proposed Mojave–Sonora Megashear of Silver and Anderson (1974).

To test the validity of Mukasa et al.'s (1984), James' (1986), and James and Mattinson's (1988) findings for the schist terrane in its entirety (Fig. 1), we undertook a regionally comprehensive U-Pb age analysis of detrital zircons from the schist (see also Jacobson et al. [2000] and Barth et al. [2003a]). Provided that U-Pb systematics in the detrital zircons were not disturbed by metamorphism, the youngest U-Pb zircon ages place an upper limit upon the depositional age while the overall age distribution yields a measure of provenance. Earlier reconnaissance

M. Grove et al.

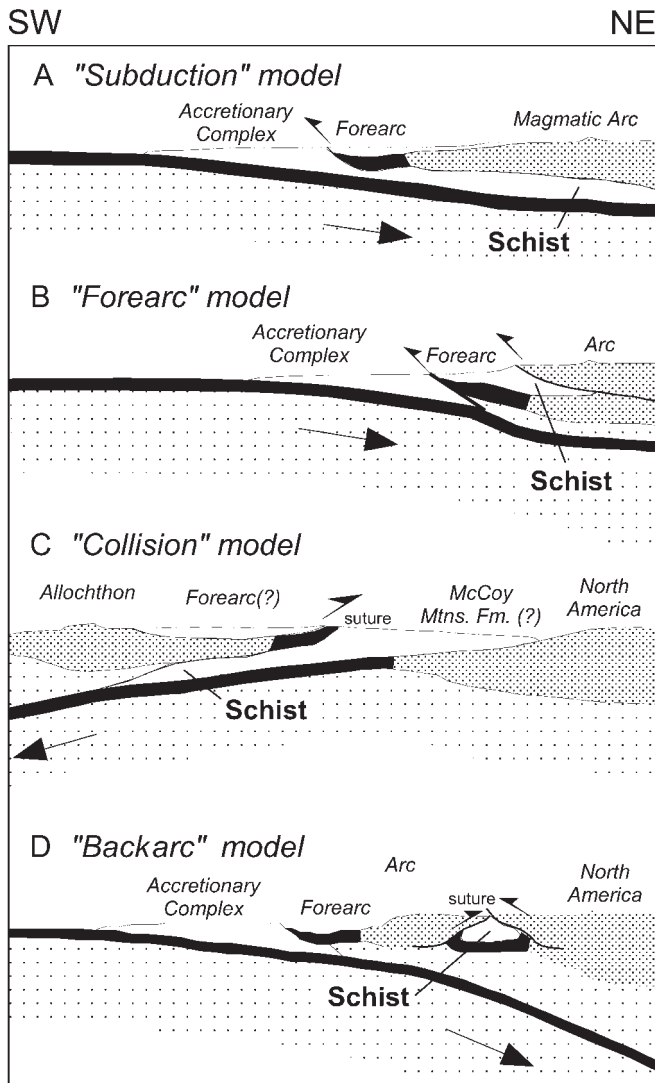SW   NE

Figure 2 Tectonic models for origin of Pelona and related schists. A: In subduction model, schist's graywacke protolith is deposited in trench, subducted, and accreted beneath tectonically eroded cratonal rocks. Lithospheric mantle has been completely removed by this process. B: In forearc model, sediments in forearc basin are overthrust by magmatic arc; C: In collision model, schist's protolith is overthrust by a northeast-directed allochthon. D: In backarc model, protolith of schist originates in a backarc basin that is subsequently overthrust and closed.

multigrain U-Pb analysis of zircons from the schist performed by Silver et al. (1984) and James and Mattinson (1988) were equivocal with respect to the depositional age of the graywacke protolith. In contrast, our initial ion microprobe results clearly indicated the presence of Late Cretaceous detritus (Jacobson et al., 2000; Barth et al., 2003a). In this paper, we present a much more comprehensive data set involving 40 samples that represent virtually all of the major schist exposures. This compilation, which includes six samples from Jacobson et al. (2000) and Barth et al. (2003a), confirms a Late Cretaceous to earliest Tertiary

depositional age for the graywacke protolith for all of the schists and reveal systematic regional variations in the depositional age and provenance of the protolith.

When combined with ^{40}Ar/^{39}Ar cooling ages, our detrital zircon U-Pb data can be used to constrain the "cycling interval" during which the schist's graywacke protolith was eroded from its source region, deposited, underthrust, accreted, and metamorphosed beneath crystalline rocks of southwestern North America. Combined with previously obtained data, new muscovite and biotite ^{40}Ar/^{39}Ar cooling ages from our detrital zircon samples clearly indicate that the cycling interval for erosion, deposition, underthrusting, accretion, and metamorphism varied systematically across the schist terrane. Schist located outboard of the craton in the southern Coast Ranges and northwestern Mojave Desert was emplaced well before schists were underplated beneath more cratonal (and progressively more southeasterly) positions in the Transverse Ranges and southeastern California and southwestern Arizona. This spatial-temporal relationship and the overall Laramide depositional age for the schist's graywacke protolith must be explained by any model that seeks to describe the underplating of the schists beneath southwest North America.

CORRELATION OF THE SCHISTS

Early attempts to correlate the Pelona, Orocopia, Rand, Portal Ridge, and Sierra de Salinas Schists (Fig. 1) were based on their field and petrographic characteristics (Ehlig, 1958, 1968). A key observation is that relative proportions of the major rock types are broadly similar in all areas (~90–99% metagraywacke, 1–10% mid-ocean ridge basalt (MORB) metabasite, and trace amounts of Fe-Mn metachert, marble, and serpentinite; Haxel and Dillon, 1978; Haxel et al., 1987, 2002; Dawson and Jacobson, 1989). Moreover, many of the schist bodies exhibit inverted metamorphic zonation; i.e., peak temperature of metamorphism decreases structurally downward (Ehlig, 1958; Graham and England, 1976; Jacobson, 1983b, 1995). In addition, the schists share a number of diagnostic mineralogic features (Haxel and Dillon, 1978): (1) poikiloblasts of sodic plagioclase in metagraywacke that appear gray to black due to inclusions of graphite; (2) local centimeter-scale clots of fuchsite in metagraywacke; (3) centimeter- to meter-scale lenses of talc-actinolite rock in metagraywacke; (4) sodic-calcic amphibole (winchite to barroisite) in low-grade metabasites; and (5) spessartine garnet, piemontite, stipnomelane, and sodic amphibole in Fe-Mn metachert.

The approximate early Tertiary positions of schist outcrops are indicated in Figure 3. Correlation among the various schists has been most readily accepted for the Pelona and Orocopia Schists, which were in close proximity prior to offset on the San Andreas system (Fig. 3; James and Mattinson, 1988; Dillon et al., 1990). Less well established is the relationship of the Pelona–Orocopia schists to the Rand Schist, schist of Portal Ridge, and schist of Sierra de Salinas.

While the Rand Schist exhibits all the key lithologic attributes of the Pelona and Orocopia Schists (Jacobson, 1995), it
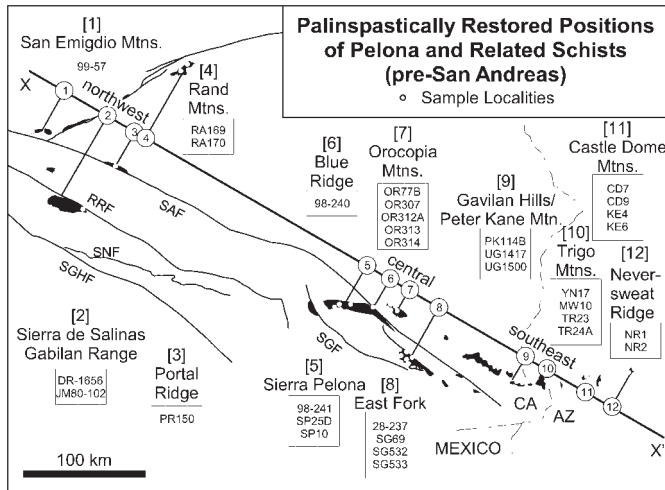
Figure 3. Sample positions plotted on a palinspastically restored base map showing pre–Late Tertiary positions of Pelona and related schist exposures of southern California and southwestern Arizona. Appendix 1 describes how this base map was constructed. Distances along projection line are used in Figure 7. Numbers (1–12) refer to geographic areas sampled in this study (see Table 1). Northwest, central, and southeast refer to three major groupings discussed in text. Abbreviations of fault names are same as in Figure 1.

differs in two respects. Some Rand metagraywackes are more aluminous than any bulk compositions observed in the Pelona and Orocopia Schists (Jacobson et al., 1988). Moreover, as indicated by initial radiometric dating (Kistler and Peterman, 1978; Silver and Nourse, 1986; Jacobson, 1990) and confirmed here, the Rand Schist is older than the Pelona and Orocopia Schists. This age difference and the spatial separation prior to offset on the San Andreas system (Fig. 3) make it difficult to know the exact paleogeographic relationships between the northern and southern schist bodies.

The schists of Sierra de Salinas and Portal Ridge have been correlated with each other on the basis of lithologic similarity and close proximity prior to slip on the San Andreas system (Ross, 1976). While a correlation to the Pelona, Orocopia, and Rand Schists was deemed unlikely by James and Mattinson (1988), other workers (e.g., Haxel and Dillon, 1978) concluded that the schists of Sierra de Salinas and Portal Ridge were simply higher-grade lithologic equivalents of the other schists. Both the schists of Sierra de Salinas and Portal Ridge were metamorphosed in the middle to upper amphibolite facies (Evans, 1966; Ross, 1976). Because they generally lack graphitic plagioclase poikiloblasts and possess a high ratio of biotite to muscovite, the schists of Sierra de Salinas and Portal Ridge typically appear quite different in outcrop than lower-grade schists found elsewhere. While we have not examined the schists of Sierra de Salinas in detail, our work in the Portal Ridge area has revealed the same talc-actinolite lenses, piemontite-bearing metachert, and other features indicative of the schist's eugeoclinal protolith. Hence, we see no reason that the schists of

Sierra de Salinas and Portal Ridge should not be lithologically correlated with the Pelona, Orocopia, and Rand Schists.

METHODS

We sampled metagraywacke from most of the significant schist exposures in southern California and southwestern Arizona (Fig. 3, Table 1; see also Jacobson et al., 2000; Barth et al., 2003a). Brief descriptions of each of the 12 sampling areas are provided in Appendix 2. The sample suite represent the range of geologic attributes (metamorphic grade, structural position, lithology) exhibited by the metagraywacke throughout the region (Table 1). In addition, many samples were selected from outcrops containing metabasite. Contacts between metagraywacke and metabasite could originally have been either tectonic or depositional. In the latter case, graywacke spatially associated with metabasite potentially represents the lowermost and oldest part of the stratigraphic section. Details of the U-Pb and $^{40}Ar/^{39}Ar$ analysis we have employed are provided in Appendices 3 and 4, respectively.

Ion Microprobe U-Pb

The efficiency of the ion microprobe (high analysis throughput with no wet chemical separation of Pb, U, and Th required) and its ability to provide high spatial resolution have resulted in the extensive use of this instrument in detrital zircon U-Pb studies over the past 20 years (Froude et al., 1983; Ireland, 1992; Maas et al., 1992; Lee et al., 1997; Miller et al., 1998; DeGraaff Surpless et al., 2002). Because small amounts of zircon are analyzed (< 1 ng), ion microprobe results are less prone (relative to isotope dilution methods) to be biased by Pb-enriched restitic regions that are likely to be present within some of our grains (e.g., Silver et al., 1984; James and Mattinson, 1988). Reduced precision accompanies smaller sample size, however, and it is generally difficult or impossible to convincingly demonstrate U-Pb concordance of spot analyses from relatively U-poor and/or young zircons. This difficulty applies to the majority of U-Pb results we produced in this study. Only Cretaceous grains with uncharacteristically high U abundances (higher than about 1500 ppm) yield sufficiently precise $^{207}Pb/^{235}U$ results that U-Pb concordance can be convincingly assessed. In most instances, our interpretations are based solely upon the more precisely determined $^{206}Pb/^{238}U$ ages.

Interpretation of detrital zircon U-Pb results from metamorphosed rocks depend significantly upon the extent to which grains examined are affected by Pb loss and/or recrystallization effects. Recent high-temperature experimental diffusion studies have indicated that Pb should be essentially immobile in crystalline zircon under crustal conditions (e.g., Cherniak and Watson, 2000). Problems arise when significant radiation damage or metamorphic zircon growth has occurred. Poorly crystalline zircon that has interacted with fluids produced at metamorphic conditions relevant to the schists is known to be prone to significant Pb loss and/or recrystallization (Pidgeon et al., 1966; Sinha et al.,

TABLE 1. SAMPLE INFORMATION

Sample	Locality	Type[†]	Area[§]	Group[#]	UTM-x[****]	UTM-y[****]	Grade[††]	Level[§§]	Mafic[##]	Plutons[***]
99-57[§§§]	San Emigdio Mts.	RS	1	NW	307.173	3860.678	A	-	-	-
JM80-102[†††]	Gabilan Range	SS	2	NW	-	-	A	-	-	-
DR-1656	Sierra de Salinas	SS	2	NW	-	-	A	-	-	-
PR150	Portal Ridge	PRS	3	NW	386.955	3830.870	A	-	-	-
RA169	Rand Mtns.	RS	4	NW	435.621	3912.289	EB	low	-	-
RA170	Rand Mtns.	RS	4	NW	431.438	3909.618	AEA	high	-	-
98-241	Sierra Pelona	PS	5	C	367.073	3821.369	GS	Int.	-	-
SP10	Sierra Pelona	PS	5	C	369.567	3822.959	GS	low	X	-
SP25D	Sierra Pelona	PS	5	C	371.584	3825.297	GS	low	X	-
98-240	Blue Ridge	PS	6	C	431.487	3803.663	AEA	-	-	-
OR77B	Orocopia Mtns.	OS	7	C	613.409	3714.761	LA	high	X	-
OR307	Orocopia Mtns.	OS	7	C	610.924	3717.529	LA	high	X	-
OR312A	Orocopia Mtns.	OS	7	C	-	-	AEA	low	-	-
OR313	Orocopia Mtns.	OS	7	C	-	-	AEA	low	-	-
OR314	Orocopia Mtns.	OS	7	C	-	-	AEA	low	-	-
98-237	East Fork	PS	8	C	431.641	3802.224	UGS	high	X	-
SG69	East Fork	PS	8	C	431.551	3793.948	UGS	high	X	-
SG532	East Fork	PS	8	C	433.398	3800.745	GS	Int.	-	-
SG533	East Fork	PS	8	C	444.292	3795.208	LGS	low	-	-
PK114B	Peter Kane Mtns.	OS	9	SE	703.878	3659.663	LA	high	-	X
UG1417A	Gavilan Hills	OS	9	SE	710.524	3653.248	LA	low	-	-
UG1500	Gavilan Hills	OS	9	SE	712.678	3653.28	LA	low	X	-
YN17	Little Picacho Wash	OS	10	SE	720.800	3653.598	AEA	-	-	-
MW10	Marcus Wash	OS	10	SE	725.790	3654.909	AEA	-	-	-
TR23	Trigo Mtns.	OS	10	SE	726.889	3658.508	AEA	-	X[###]	-
TR24A	Trigo Mtns.	OS	10	SE	729.928	3658.508	AEA	-	X[###]	-
CD7	Castle Dome Mtns.	OS	11	SE	765.922	3658.934	LA	-	-	X
CD9	Castle Dome Mtns.	OS	11	SE	765.636	3659.319	LA	-	-	X
KE4	Castle Dome Mtns.	OS	11	SE	776.537	3656.621	LA	-	-	-
KE6	Castle Dome Mtns.	OS	11	SE	775.745	3655.262	LA	-	-	-
NR1	Neversweat Ridge	OS	12	SE	240.274	3662.994	LA	-	-	X
NR2	Neversweat Ridge	OS	12	SE	240.443	3663.413	LA	-	-	X

[†]SS—schist of Sierra de Salinas; RS—Rand Schist; PRS—schist of Portal Ridge; PS—Pelona Schist; OS—Orocopia Schist.
[§]12 area subdivisions employed in text.
[#]NW—northwest, C—central, SE—southeast.
[††]Metamorphic grade: EB—epidote blueschist; GS—greenschist, AEA—albite epidote amphibolite, A—amphibolite (L—lower, U—upper).
[§§]Structural level: low—structurally deep; int.—structurally intermediate; high—near upper low-angle fault contact.
[##]"x" denotes sample collected adjacent to mafic schist and/or metachert.
[***]"x" denotes potential contact metamorphism due to nearby igneous bodies.
[†††]Sample studied by James and Mattinson (1988).
[§§§]Locality studied by James (1986).
[###]Field relations of metadiorite are similar to body studied by Mukasa et al. (1984).
[****]UTM coordinates are zone 11 (except Neversweat Ridge is zone 12).

1992; Mezger and Krogstad, 1997; Geisler et al., 2001; Högdahl et al., 2001). In general, the extent of radiation damage depends most strongly upon uranium content and age. Hence, there are obvious tests for such problematic behavior. If, for example, zircons yielding the youngest U-Pb ages were systematically found to possess the highest U-contents, then Pb loss would be identified as a potentially serious problem. Another useful test is to examine the relationship between U-Pb age and Th/U. Metamorphic overgrowths on igneous zircons are often characterized by very low Th/U (Kröner et al., 1994; Carson et al., 2002; Mojzsis and Harrison, 2002; Rubatto, 2002). Consequently, if the youngest detrital zircon U-Pb ages were highly correlated with anomalously low Th/U values, then growth of metamorphic zircon should be suspected to have played a prominent role in producing these young ages.

$^{40}Ar/^{39}Ar$

Muscovite and/or biotite ages were obtained from most of the detrital zircon samples (Table 1). Because the schist was so extensively recrystallized at upper greenschist to amphibolite facies conditions, it is extremely unlikely that any detrital micas survived metamorphism. Available petrographic and compositional data from the phengitic white mica and biotite present within the schist confirm that they are metamorphic phases (Jacobson, 1983b, 1990, 1995, 1997; Jacobson et al., 1988, 2002a). When transient heating is unimportant and incorporation of excess radiogenic ^{40}Ar is not a factor, $^{40}Ar/^{39}Ar$ ages from metamorphic micas will record post-metamorphic cooling through their bulk closure temperature (McDougall and Harrison, 1999). Under these conditions, the cycling interval during which the schist's graywacke protolith was eroded from its source region, deposited, underthrust, accreted, and metamorphosed will be bracketed between the youngest detrital U-Pb zircon ages and post-metamorphic $^{40}Ar/^{39}Ar$ cooling ages recorded by the micas.

Because age spectra yielded by biotite and, to a lesser extent, muscovite are degraded by the dehydroxylation processes during *in vacuo* step-heating (McDougall and Harrison, 1999), thermal history information from micas is most reliably obtained from total gas $^{40}Ar/^{39}Ar$ ages that can be related to bulk closure temperatures. Although the latter are not well determined, available empirical and experimental data indicate bulk closure temperatures of ~400 °C for muscovite and 350 °C for biotite (McDougall and Harrison, 1999) for geologically reasonable cooling rates and diffusive length scales.

RESULTS

U-Pb zircon

Analytical Considerations

Analytical uncertainties in $^{206}Pb/^{238}U$ age for unknowns averaged 2.7% throughout our study[1]. This quantity is similar in magnitude to the spot-to-spot reproducibility predicted by the scatter

of calibration data defining the calibration (3.1%, N = 272; see Appendix 3). Average radiogenic yields for ^{206}Pb and ^{207}Pb were 95.9% and 72.1%, respectively. The far more significant common lead corrections that were applied to measured ^{207}Pb caused errors associated with $^{207}Pb/^{235}U$ ages to be, on average, six times greater than those of corresponding $^{206}Pb/^{238}U$ ages (Fig. 4; see Appendix 3). The large uncertainties in $^{207}Pb/^{235}U$ age generally compromised our ability to evaluate results for U-Pb discordance and required our interpretations to be based primarily upon $^{206}Pb/^{238}U$ ages. In 14% of our measurements, $^{206}Pb/^{238}U$ and $^{207}Pb/^{235}U$ ages were distinguishable at the 1σ level. In most of these cases (11% of total), the U-Pb ages were sufficiently old (generally greater than 1 Ga) that well determined $^{207}Pb/^{206}Pb$ ages were calculated. Since $^{207}Pb/^{206}Pb$ ages are more reliable than U-Pb ages for approximating the time of crystallization of zircons that have experienced Pb loss, we used them in lieu of $^{206}Pb/^{238}U$ ages in the cases where they could be precisely measured. While our use of $^{206}Pb/^{238}U$ ages for the remaining discordant analyses (3% of total) is potentially problematic, it does not bias the remaining data in any systematic way. In fact, we will show that the overall U-Pb age distributions we obtained from the schist are extremely coherent on a regional scale and similar to those exhibited by the likely protolith (DeGraaff Surpless et al., 2002; Jacobson et al., 2002b).

Abundance of Late Cretaceous Zircons

Our detrital zircon U-Pb results are summarized in Table 2. The most fundamental outcome of this study is that Late Cretaceous $^{206}Pb/^{238}U$ ages were measured in at least one grain in 37 of the samples examined, with the remaining two samples giving ages as young as late Early Cretaceous (Table 2). This occurred in spite of the fact that fewer than 15 grains were measured for 60% of the samples. In fact, 42% of the grains yielded $^{206}Pb/^{238}U$ ages less than 100 Ma while an additional 20% of the results were Early Cretaceous (Table 2).

The relevance of the Late Cretaceous zircon U-Pb ages for the age of the schist's sedimentary protolith could be questioned if the detrital zircons experienced Pb loss or were overgrown by metamorphic zircon during upper greenschist to amphibolite facies recrystallization that attended underthrusting. Petrographic inspection and limited cathodoluminescence (CL) imaging (Jacobson et al., 2000) indicate that most samples we examined contain abundant euhedral to partially rounded zircons with characteristically simple oscillatory zoning patterns that we interpret as magmatic features. These characteristics make it seem most reasonable to us that the vast majority of our U-Pb ages represent igneous recrystallization ages.

Barth et al. (2003a) carefully integrated CL imaging and ion probe U-Pb study of detrital zircons from the comparatively high
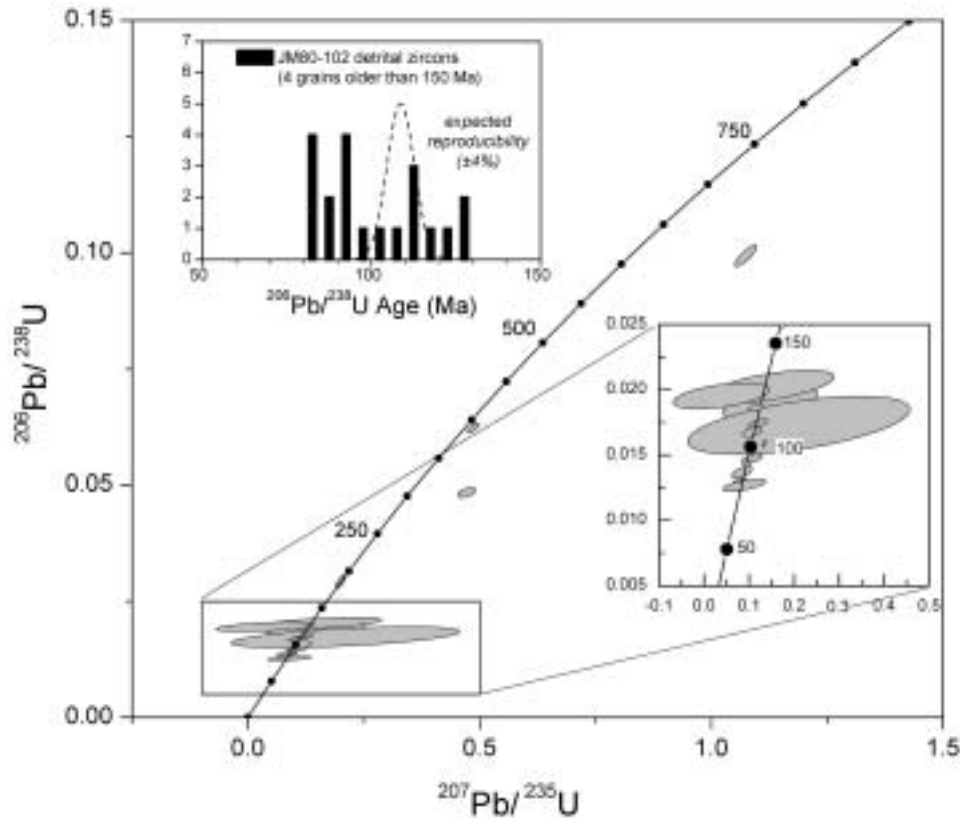
M. Grove et al.

Figure 4. Representative concordia plot from JM80-102. Upper inset is histogram of results from 50 to 150 Ma. Four of 23 results plot outside this range. Gaussian curve represents expected spot-to-spot reproducibility based upon measurements of AS-3 standard zircon. Lower inset is a vertically expanded view of concordia.

grade schist of Sierra de Salinas (see Table 1), which locally contains sillimanite (Ross, 1976) and hence indicates significantly higher peak metamorphic temperatures than were attained in most other bodies of the schist. They determined that thin (1–15 μm), CL bright, low Th/U overgrowths of potential metamorphic origin were present on a number of grains. While these have proven difficult to measure directly in conventionally sectioned and polished grains, we cannot preclude the possibility that some of our zircon U-Pb analyses are anomalously young because the beam overlapped metamorphic zircon.

Because metamorphic overgrowths on igneous zircons generally have very low Th/U (Kröner et al., 1994; Rubatto, 2002; Carson et al., 2002; Mojzsis and Harrison, 2002), we can make some inferences about the extent to which anomalously young ages produced by metamorphic overgrowths influence our results by examining the U-content and Th/U versus U-Pb age for our zircons (Fig. 5). As indicated, there is no clear relationship between U-Pb age and either U or Th/U (note that Th was not determined in 25% of the analyses). To illustrate this, we have used a filled symbol to represent the youngest age measured in each of the samples in Figure 5. As shown, spot analyses from most of these grains define essentially the same range of U concentrations (50–5000 ppm) and Th/U (0.05–1.5) as those exhibited by Proterozoic grains that are the most susceptible to Pb loss by virtue of protracted exposure to radiation damage. Roughly 88% of our results yield Th/U ratios greater than the values (<~0.1) that are

believed suggestive of metamorphic zircon (Kröner et al., 1994; Rubatto, 2002; Carson et al., 2002; Mojzsis and Harrison, 2002). In five of our samples, the youngest zircon ages also have Th/U values below 0.1. (see also Barth et al., 2003a). These included an 80 Ma result with Th/U = 0.009 from JM80–102 (Gabilan Range) and a 59 Ma result with Th/U = 0.028 from TR23 (Trigo Mountains). In both cases, however, the next oldest grains were only slightly older (81 Ma in JM80–102 and 67 Ma in TR23) and had Th/U in excess of 0.1. Moreover, the youngest U-Pb age we measured (a 55 Ma result from Neversweat Ridge) had Th/U = 0.25 and less than 200 ppm U. Hence, while it is likely that limited metamorphic zircon growth has influenced our results, there is no obvious evidence that it impacts them in a serious way.

Provenance Analysis

In the initial stages of the study, we analyzed 30–50 grains per sample. Subsequently, our efforts to detect whether or not Late Cretaceous grains were present in as many samples as possible motivated us to greatly reduce the number of grains analyzed per sample (to as few as 10). Such a limited sampling rate is significantly less than that required for a statistically meaningful age distribution (e.g., Dodson et al., 1988). Inspection of Table 2 reveals that closely spaced samples from a single area can differ quite dramatically in their distribution of detrital ages. Hence, it is clearly desirable to combine data from adjacent samples to ensure that the overall variability from a given

Temporal and spatial trends of Late Cretaceous–early Tertiary underplating   9

TABLE 2. SUMMARY OF U-Pb AGE* RESULTS FROM DETRITAL ZIRCONS

Sample	Area[§]	Group[§]	N[#]	Age Bins**							
				Late K[††]	Early K[††]	55–70 (Ma)	71–80 (Ma)	81–90 (Ma)	91–145 (Ma)	146–248 (Ma)	>249 (Ma)
99-57	1	NW	35	8	22	-	-	-	30	3	2
JM80-102	2	NW	23	9	7	-	-	6	10	2	5
DR-1656	2	NW	28	11	7	-	1	5	12	2	8
PR150	3	NW	40	19	9	-	6	6	22	5	7
RA169	4	NW	46	17	16	-	1	5	27	7	6
RA170	4	NW	39	17	15	-	1	2	29	1	6
98-241[†]	5	C	50	28	-	2	10	14	2	5	17
SP10	5	C	10	8	2	-	-	-	10	-	-
SP25D	5	C	10	7	3	-	1	1	8	-	-
98-240[†]	6	C	43	17	22	-	-	5	34	3	1
OR77B	7	C	11	4	3	-	-	2	5	-	4
OR307	7	C	14	4	2	-	-	-	6	3	5
OR312A	7	C	10	2	-	-	-	2	-	3	5
OR313	7	C	9	1	1	-	-	-	2	2	5
OR314	7	C	13	3	-	-	-	2	1	3	7
98-237	8	C	31	20	5	-	1	13	11	4	2
SG69	8	C	10	3	1	-	-	2	2	4	2
SG532	8	C	10	6	-	-	5	-	1	-	4
SG533	8	C	32	20	4	1	9	7	7	4	4
PK114B	9	SE	11	8	3	-	4	3	4	-	-
UG1417A[†]	9	SE	45	32	2	-	18	11	5	1	10
UG1500	9	SE	10	-	5	-	-	-	5	1	4
YN17	10	SE	14	1	-	-	-	-	1	5	8
MW10	10	SE	13	3	-	-	1	1	1	4	6
TR23	10	SE	17	7	8	3	-	2	10	2	-
TR24A	10	SE	17	3	2	1	-	2	2	6	6
CD7	11	SE	33	4	1	-	2	-	3	8	20
CD9	11	SE	10	1	-	-	1	-	-	2	7
KE4	11	SE	12	2	1	-	-	-	1	4	5
KE6	11	SE	18	7	1	1	1	5	1	5	5
NR1	12	SE	11	6	1	1	3	1	2	1	2
NR2	12	SE	35	24	2	12	8	4	2	3	6

*Statistically concordant results (86% of 710 analyses) represented by ^{206}Pb/^{238}U ages. Discordant analyses that were sufficiently old (i.e., > 1 Ga; 11% of 710 analyses) have been represented by ^{207}Pb/^{206}Pb ages. Remainder (3%) are generally Cretaceous and are represented by ^{206}Pb/^{238}U ages.
[†]Results from Jacobson et al. (2000).
[§]See Table 1 and Appendix 1 for further details.
[#]Total spot analyses obtained per sample (one spot analysis per grain).
**Numbers represent quantity of analyses that fall within indicated age bins.
[††]Early Cretaceous (Early K) is 100–145 Ma, Late Cretaceous (Late K) is 6–100 Ma

region is adequately represented. To accomplish this, we pooled results at two different scales. At the local level, we combined samples from individual schist bodies or adjacent schist bodies as indicated in Figure 3 (see Table 2). At a more regional scale, we pooled our results into three groups based upon their palinspastically restored positions: (1) samples from the Rand Schist and the schists of Sierra de Salinas and Portal Ridge defined a "northwest" group; (2) samples of the Pelona Schist and the Orocopia

Schist of the Orocopia Mountains defined a "central" group; and (3) all bodies of Orocopia Schist southeast of the Orocopia Mountains defined a "southeast" group.

We employed the following age bins in our analysis: 55–70 Ma, 71–80 Ma, 81–90 Ma, 91–145 Ma, 146–248 Ma (i.e., Jurassic and Triassic), and 249–2000 Ma (Paleozoic to middle Early Proterozoic). The comparatively fine subdivision of the Cretaceous is justified since nearly two-thirds of our detrital
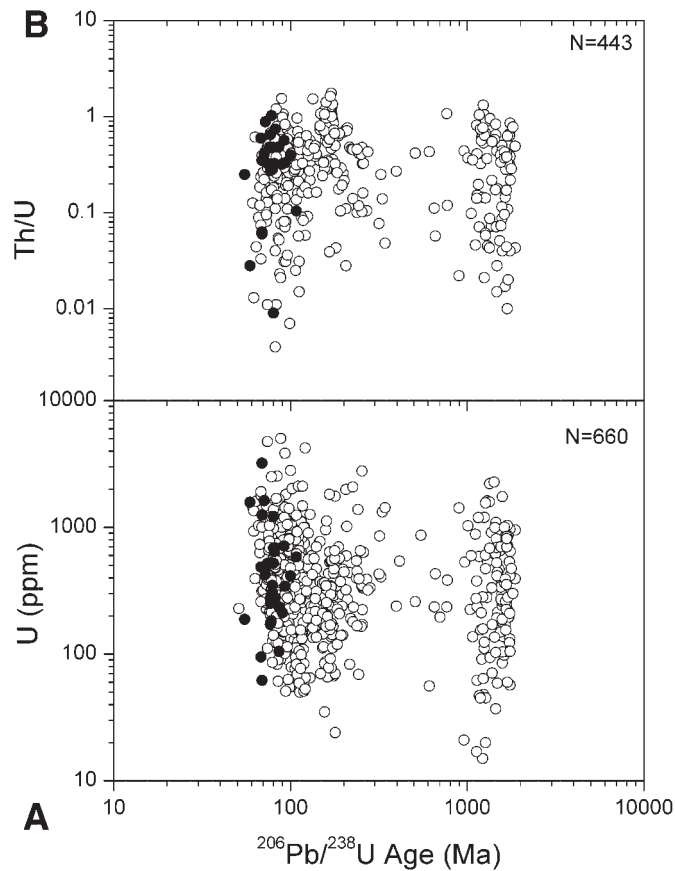
Figure 5. A: U-content versus U-Pb age; B: Th/U versus U-Pb age. Filled symbols indicate youngest ^{206}Pb/^{238}U age obtained each of 40 samples (includes data from Jacobson et al., [2000] and Barth et al., [2003a]). Note that Cretaceous results exhibit same range of U and Th/U as grains that have preserved Proterozoic U-Pb ages. This is evidence against preferential Pb loss by Cretaceous grains. Dashed line indicates lower limit of Th/U values (0.10 ± 0.05) yielded by zircons from greywackes of the Great Valley Group (DeGraaff Surpless et al., 2002). By this standard, metagraywacke zircon Th/U values less than 0.1 are anomalously low and may signal metamorphic zircon growth.
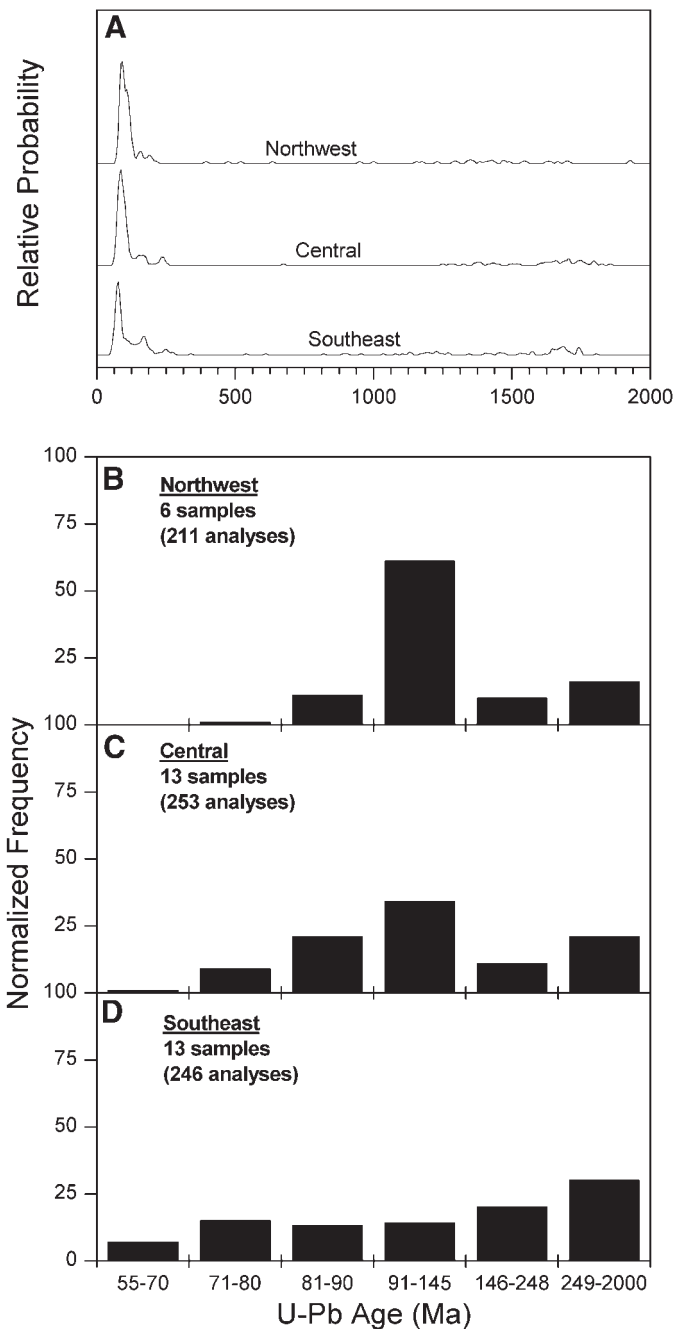

Figure 6. A: U-Pb age frequency spectra for northwest schists (Rand Schist and schists of Portal Ridge and Sierra de Salinas), central schists (Pelona Schist and Orocopia Schist of Orocopia Mountains), and southeastern schists (Orocopia Schist excluding that exposed in Orocopia Mountains). All three geographic groups contain subequal proportions of Mesozoic (dominantly Cretaceous) and late Early to late Middle Proterozoic grains. Normalized histograms of U-Pb ages from (B) northwest, (C) central, and (D) southeast schists shown in (B), (C), and (D), show that progressive decrease of maximum possible depositional age of graywacke protolith from northwest to southeast (in palinspastically restored coordinates) is accompanied by prominent change in provenance.

zircon U-Pb data ages are Cretaceous. Moreover, as will be evident below, it facilitates comparison to potential source regions of southwestern North America. We combined all Jurassic and Triassic ages into the same bin, since crystalline rocks of this age tend to occur in the same areas. Also note that, while we put all pre-Mesozoic results into a single bin, only about 4% of these are between 249 and 1100 Ma. Moreover, most of the 249–1100 Ma ^{206}Pb/^{238}U ages obtained were yielded by grains that exhibit U-Pb discordance at the 1σ level. Hence the 249–2000 Ma bin is populated primarily by late Early Proterozoic to earliest Late Proterozoic zircons.

Zircon U-Pb age distributions from the three major geographic groups discussed above are plotted in Figure 6. The relative probability plots of Figure 6A clearly demonstrate the abun-

dance of Cretaceous ages. When the age bins defined above are employed, it becomes evident that Early to early Late Cretaceous (91–145 Ma) zircons overwhelmingly populate samples from the northwest schist exposures (Fig. 6B), whereas subequal proportions of Proterozoic, Triassic/Jurassic, and latest Cretaceous to earliest Tertiary zircons typify detrital zircon populations within the southeast schist exposures (Fig. 6D). The central group is transitional between the other two (Fig. 6C). Note that the proportion of Cretaceous zircons decreases sharply from 69% in the northwest to 48% in the southeast. This falloff is primarily an expression of the proportion of 91–145 Ma zircons in the northwest present (compare parts B and D in Fig. 6). Zircons in this age range constitute 55% of the population in the northwest but only 16% of the population in the southeast. At the same time, the proportion of Jurassic and Triassic grains increases significantly in the southeast. Paleozoic and latest Proterozoic grains are very sparse in all samples (Fig. 6A).

A second important trend is the systematic southeastward decrease in U-Pb ages of the youngest zircons (Fig. 6, B–D). For example, 13% of the grains from the Schist of Sierra de Salinas and the Rand Schist fall in the 80–90 Ma range while an additional 1.3% of the results are as young as 77 Ma (Fig. 6B). In the central region, 13% of the zircon analyses of Pelona Schist fall in the 71–80 Ma range while an additional 1.3% of the results are as young as 68 Ma (Fig. 6C). Finally, 7% of the zircon ages from the schists of the southeastern region are in the 55–70 Ma range (1% are less than 60 Ma) (Fig. 6D). Because the accuracy of our $^{206}Pb/^{238}U$ ages is on the order of 3% (see Appendix 3), the very youngest ages in each of the three groupings could reasonably be ascribed to analytical scatter. However, the large numbers of grains with slightly older ages cannot be easily dismissed as measurement artifacts and strongly imply that systematically younger detrital zircons are present to the southeast.

^{40}Ar/^{39}Ar Thermal History Results

Muscovite and biotite ^{40}Ar/^{39}Ar age spectra measured in this study (complete ^{40}Ar/^{39}Ar data tables and derivative plots are available from the GSA Data Repository; see footnote 1) all revealed monotonically increasing age gradients at low-temperature gas release. This pattern typifies metamorphic micas from slowly cooled, deep-seated subduction settings (e.g., Grove and Bebout, 1995). In general, there was no indication of excess ^{40}Ar. One sample (SG532A muscovite) did yield an initially old step indicative of excess ^{40}Ar that constituted less than 1% ^{39}Ar release in the age spectrum. In addition, the age spectra of several samples that were run sequentially yielded zero ages during the initial 1% of ^{39}Ar release (KE1 biotite, OR312A biotite, OR314 biotite, PR36A muscovite, and TR18 muscovite). We attribute these initial zero ages to unresolved hydrocarbon interferences at mass 36 that resulted from an under-performing getter pump. Neglecting these problematic initial steps, we calculated bulk closure ages and interpreted the results as indicating the time of post-metamorphic cooling. Results are summarized in Table 3.

Muscovite post-metamorphic cooling ages decrease systematically from 90 Ma in the northwest (San Emigdio Mountains) to 40 Ma in the southeast (Neversweat Ridge; Fig. 7). Although data are less abundant for biotite, a second pattern is also evident in Figure 7. Specifically, biotite is only 2–3 m.y. younger than muscovite in the San Emigdio Mountains and the western Mojave region but up to 20 m.y. younger than muscovite in southeastern California and southwestern Arizona. While we cannot absolutely rule out reheating effects related to Tertiary volcanism or hypabyssal plutonism in the Castle Dome Mountains or Neversweat Ridge area (see Appendix 2), virtually identical muscovite and biotite ages were obtained from the Trigo Mountains, which show relatively little Tertiary intrusion. Consequently, we believe

TABLE 3. ^{40}Ar/^{39}Ar MICA TOTAL GAS AGES*

| Sample	Locality	Mus	Bio
9957	San Emigdio Mtns.	89.8 ± 0.2	86.1 ± 0.2
RA83	Rand Mtns.	74.2 ± 0.2	-
RA100	Rand Mtns.	69.8 ± 0.2	-
RA138	Rand Mtns.	67.4 ± 0.2	-
RA85	Rand Mtns.	67.8 ± 0.2	-
PR36	Portal Ridge	69.6 ± 0.1	67.1 ± 0.6
PR150	Portal Ridge	65.5 ± 0.2	-
98241	Sierra Pelona	58.5 ± 0.1	-
SP25D	Sierra Pelona	51.8 ± 0.2	-
SP10	Sierra Pelona	57.8 ± 0.1	-
98240	San Gabriel Mtns. (BR)	48.8 ± 0.2	-
SG43	San Gabriel Mtns. (EF)	51.4 ± 0.2	-
SG69	San Gabriel Mtns. (EF)	57.8 ± 0.1	-
SG81	San Gabriel Mtns. (EF)	52.8 ± 0.1	-
98237	San Gabriel Mtns. (EF)	55.5 ± 0.3	-
SG530	San Gabriel Mtns. (EF)	42.2 ± 0.1	-
SG531	San Gabriel Mtns. (EF)	43.4 ± 0.2	-
SG532	San Gabriel Mtns. (EF)	34.2 ± 0.2	-
SG533	San Gabriel Mtns. (EF)	31.7 ± 0.2	-
EF421	San Gabriel Mtns. (EF)	57.5 ± 0.2	-
EF463	San Gabriel Mtns. (EF)	57.8 ± 0.2	-
EF503	San Gabriel Mtns. (EF)	53.0 ± 0.2	-
EF525	San Gabriel Mtns. (EF)	54.1 ± 0.2	-
OR77B	Orocopia Mtns.	44.6 ± 0.1	-
OR312A	Orocopia Mtns.	34.3 ± 0.6	25.3 ± 0.1
OR314	Orocopia Mtns.	42.1 ± 0.1	-
OR178	Orocopia Mtns.	42.7 ± 0.2	-
PK114B	Peter Kane Mtns.	49.0 ± 0.2	-
UG805	Gavilan Hills	49.3 ± 0.2	34.7 ± 0.2
YN17	Little Picacho Wash	44.3 ± 0.1	22.6 ± 0.4
MW10	Marcus Wash	45.6 ± 0.1	-
TR18	Trigo Mtns.	43.6 ± 0.4	-
TR24A	Trigo Mtns.	44.9 ± 0.2	-
CD9	W. Castle Dome Mtns.	41.1 ± 0.1	-
KE1	E. Castle Dome Mtns.	44.2 ± 0.1	35.8 ± 0.1
KE3	E. Castle Dome Mtns.	42.2 ± 0.1	18.9 ± 0.3
KE6	E. Castle Dome Mtns.	42.7 ± 0.1	-
NR1	Neversweat Ridge	-	19.3 ± 0.3
NR2	Neversweat Ridge	40.4 ± 0.1	-

*Italicized ages from Jacobson (1990).

M. Grove et al.
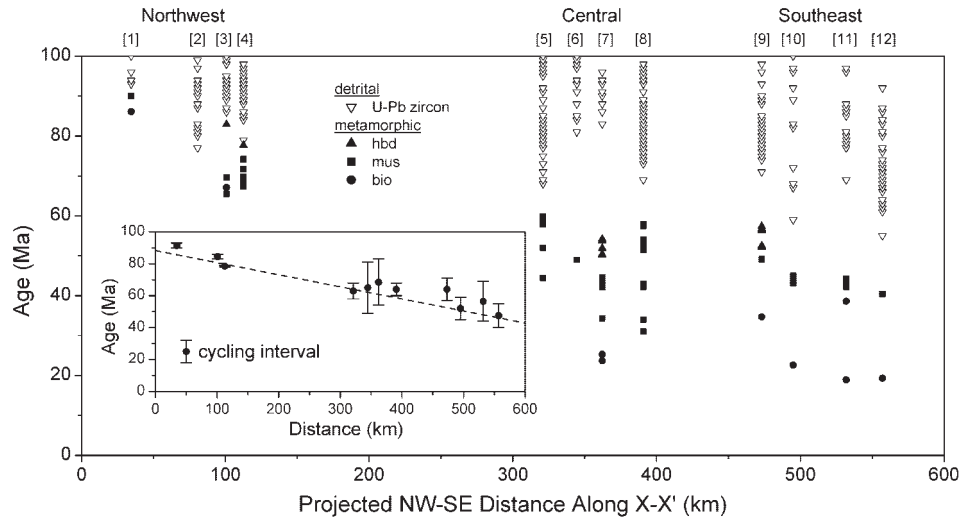
Figure 7. Summary of ^{40}Ar/^{39}Ar cooling ages and zircon U-Pb ages as function of relative northwest-southeast distance for each of 12 areas studied (see Fig. 3 for locations). Additional ^{40}Ar/^{39}Ar data from Jacobson (1990), Jacobson et al. (2002), Vucic et al. (2002), and Barth et al. (2003a) have been included in this plot. Zircons with low Th/U suggestive of metamorphic growth not been used to calculate minimum detrital age. Average time difference between youngest U-Pb detrital zircon age and oldest cooling age is 13 ± 10 Ma. During this time graywacke protolith of schist was eroded from its basement source region, deposited, underthrust, accreted, and metamorphosed.

the results are best interpreted as indicating that cooling from peak metamorphic conditions occurred earlier and more rapidly in the northwest relative to the southeast.

DISCUSSION

Time-Space Constraints upon the Evolution of the Pelona and Related Schists

Late Cretaceous–Early Tertiary Depositional Age for the Schist

The depositional age of the graywacke protolith of the schist is necessarily younger than the youngest detritus contained within it. On the basis of textural and compositional characteristics, we believe that the vast majority of detrital zircons we examined from the schist are igneous in origin. The available evidence (Fig. 5) also strongly indicates that the U-Pb ages yielded by ion probe analysis of the detrital zircons overwhelmingly represent igneous crystallization ages unaffected by Pb loss or metamorphic zircon formation during peak-grade recrystallization of the schist. Hence, the preponderance of ^{206}Pb/^{238}U ages less than 100 Ma (Table 2) requires that the depositional age of the graywacke protolith of all schist samples we examined was also Late Cretaceous or, in the case of the easternmost bodies, as young as early Tertiary. Because our sampling adequately represents the known geographic extent of the schist terrane and all variation manifested within it (Table 1), we conclude that it is highly unlikely that any portion of the schist terrane (Pelona-Orocopia-Rand-Portal Ridge-Sierra de Salinas) was formed from sedimentary sequences deposited prior to Late Cretaceous time.

Our results are in direct conflict with the conclusion of James (1986) and James and Mattinson (1988) that the Rand Schist of the San Emigdio Mountains is intruded by the 131 Ma tonalite of Antimony Peak. We analyzed 35 detrital zircon grains from one sample of the schist in this area (99–57). All ages but

five were less than 131 Ma, and all but 11 were less than 110 Ma. Based on the detrital zircon ages, our limited field observations, and the mapping of Ross (1989), we conclude that the contact between schist and tonalite in this area is a fault and that the age of the tonalite does not constrain either the depositional or metamorphic age of the schist.

Our results also contradict the inference of Mukasa et al. (1984) that a 163 Ma mafic diorite (now metamorphosed) found within the Chocolate Mountains intruded the protolith of the schist. While we were unable to analyze any samples from this locality, which lies within an active bombing range, we did examine two samples of schist adjacent to possible correlatives of the metadiorite in the Trigo Mountains (samples TR23 and TR24A; Haxel et al., 2002). The proportions of Late Cretaceous U-Pb ages yielded by detrital zircons from these samples were 41% and 18%, respectively. This result leads us to doubt the intrusive relation inferred by Mukasa et al. (1984). Instead, we suggest that the metadiorite was incorporated into the schist protolith as either a sedimentary or tectonic fragment. The 163 Ma igneous age of the metadiorite and its arc-like geochemical signature (Haxel et al., 1987, 2002) suggest a potential correlation with the Coast Range ophiolite (Dickinson et al., 1996). The Coast Range ophiolite forms the basement of the western Great Valley forearc basin. Exotic blocks of Coast Range ophiolite are inferred to be present in the Franciscan Complex (MacPherson et al., 1990) and may provide an analog for late Middle Jurassic metadiorite within the schist.

Finally, all previous reports of post-metamorphic, Late Cretaceous intrusion of the schist also appear to be incorrect. The Randsburg granodiorite within the Rand Mountains clearly intrudes the Rand Schist and has produced contact metamorphism within it (Silver and Nourse, 1986). Conventional zircon U-Pb data reported by Silver and Nourse (1986) from the pluton were interpreted as indicating a 79 ± 1 Ma crystallization age.

However, new ion microprobe U-Pb zircon and ^{40}Ar/^{39}Ar biotite and hornblende results from the Randsburg granodiorite demonstrate that it was actually emplaced during the early Miocene (Barth et al., 2003b). Hence, the intrusive relationship between the Randsburg granodiorite and Rand Schist does not place any significant constraints on the emplacement history of the schist.

Similarly, past assessments that the schist of Sierra de Salinas was intruded and contact metamorphosed during the Late Cretaceous appear to have been based upon misinterpreted geologic relationships. Granitic rocks spatially associated with the schist of Sierra de Salinas in the southern Coast Ranges comprise a diverse calc-alkalic suite (Ross, 1984) with U-Pb ages of 82–94 Ma (Mattinson, 1978, 1990; Mattinson and James, 1985; Barth et al., 2003a). While Ross and Brabb (1973) originally mapped the contacts between schist and granitic rocks as Cenozoic faults based on their generally straight trace and the lack of intrusive bodies in the schist, Ross (1976) subsequently concluded that the schist bodies in the Sierra de Salinas and Gabilan Range had been contact metamorphosed by the adjacent granitoids. The U-Pb ages of detrital zircons and the contrasting biotite ^{40}Ar/^{39}Ar cooling ages exhibited by the schist of Sierra de Salinas and adjacent granitoids (Barth et al., 2003a) clearly demonstrate that deposition of the schist's protolith postdated granitoid intrusion in the area.

Regional Variation in the Timing of Deposition, Underthrusting, and Metamorphism

Results shown in Figure 7 require that the cycling interval for the graywacke protolith of the schist (i.e., the interval during which the schist's protolith was eroded from its source region, deposited, underthrust, accreted, and metamorphosed) was generally short. As indicated in Figure 7, the upper bound of the interval is defined by the youngest detrital zircon U-Pb age while the lower bound is established by the oldest ^{40}Ar/^{39}Ar cooling age. The timing of this interval decreases from 93 to 90 Ma in the San Emigdio Mountains (southernmost Sierra Nevada) to 55–43 Ma in the Neversweat Ridge area (southwestern Arizona). Hence, the entire cycle of processes occurred earlier for the Rand Schist and the schists of Portal Ridge and Sierra de Salinas in the northwest than it did for the Pelona and Orocopia Schists situated progressively farther southeast in palinspastically restored coordinates (Fig. 3).

Our data indicate an average duration for the cycling interval of 13 ± 10 m.y. along the entire belt (see inset in Fig. 7). For the Rand Schist and schist of Portal Ridge, the cycling interval is too small to be resolved with the methods we have employed (~3 m.y.). Since our results provide only maximum and minimum bounds, the gap is likely to have been smaller than that depicted in Figure 7. This is due partly to the statistical likelihood of finding detrital zircons just older than the age of deposition. Moreover, to the extent to which the source region was plutonic, nearly synchronous intrusion and rapid exhumation are required to supply materials of appropriate age. In addition, hornblende is available from only a few localities. Muscovite ages defining

the lower bound may significantly postdate the time of peak-grade metamorphism since its closure temperature (~400 °C; McDougall and Harrison, 1999) is significantly lower than the peak metamorphic temperature in many of the areas investigated (~450–>550 °C; Graham and Powell, 1984; Jacobson, 1995). Hornblende, which is more retentive of ^{40}Ar, clearly constrains the time of peak-grade metamorphism more tightly. For example, hornblendes from Portal Ridge (83 Ma) and the Rand Mountains (78 Ma) are respectively 13 m.y. and 4 m.y. older than muscovites sampled from adjacent exposures (Jacobson, 1990). In the Gavilan Hills, hornblende total gas ages range from 52 to 58 Ma and are 3–10 m.y. older than muscovites from adjacent rocks (Jacobson et al., 2002a). These observations and the fact that terminal ages in the muscovite ^{40}Ar/^{39}Ar age spectra can be several million years older than the total gas ages reported in Table 3 indicate that the interval for deposition and accretion is likely to be well under 10 m.y. for the entire schist terrane. We are currently working to improve the database of hornblende ^{40}Ar/^{39}Ar results to confirm this.

The ^{40}Ar/^{39}Ar data collected here also have implications for the exhumation history of the schists. For example, recent work in the Gavilan Hills (Jacobson et al., 2002a) and Orocopia Mountains (Vucic et al., 2002) of southeastern California has recognized two important phases of Tertiary cooling attributed to two discrete denudation events. Closure of hornblende and muscovite occurred in the early Tertiary (between 58 and 44 Ma). Subsequent slow cooling in the temperature range corresponding to biotite closure produced a spread of biotite total gas ages from 44 to 30 Ma in the Gavilan Hills and down to 20 Ma in the Orocopia Mountains. Rapid cooling in the middle Tertiary (28–20 Ma) caused K-feldspar to close (Jacobson et al., 2002a; Vucic et al., 2002). Results shown in Figure 7 suggest that a broadly similar history may apply to rocks east of the Gavilan Hills in southwestern Arizona.

Spatial/Temporal Variation of the Provenance of the Source Region

The northwest to southeast decrease of protolith age evident in our data is accompanied by a dramatic shift in sediment provenance that closely mimics the crystallization ages of basement rocks that structurally overlie the schists. Figure 8 is a first-order palinspastic restoration showing the pre–San Andreas distribution of basement rocks of southern California and western Arizona. Figure 9 indicates the distribution of detrital zircon U-Pb ages from the same region. Comparison of Figures 8 and 9 makes it clear that the dominantly 81–145 Ma detrital zircon population from the Rand Schist and the schist of Portal Ridge and Sierra de Salinas in the northwest forms a good match to the known intrusive ages from the medial Cretaceous Sierran batholith (Stern et al., 1981; Chen and Moore, 1982; Saleeby et al., 1987; Barth et al., 2003a). Similar detrital zircon U-Pb age distributions have been measured by DeGraaff Surpless et al. (2002) from the Upper Cretaceous part of the Great Valley Group in the San Joaquin Valley and by Jacobson et al. (2002b) from Upper Cretaceous
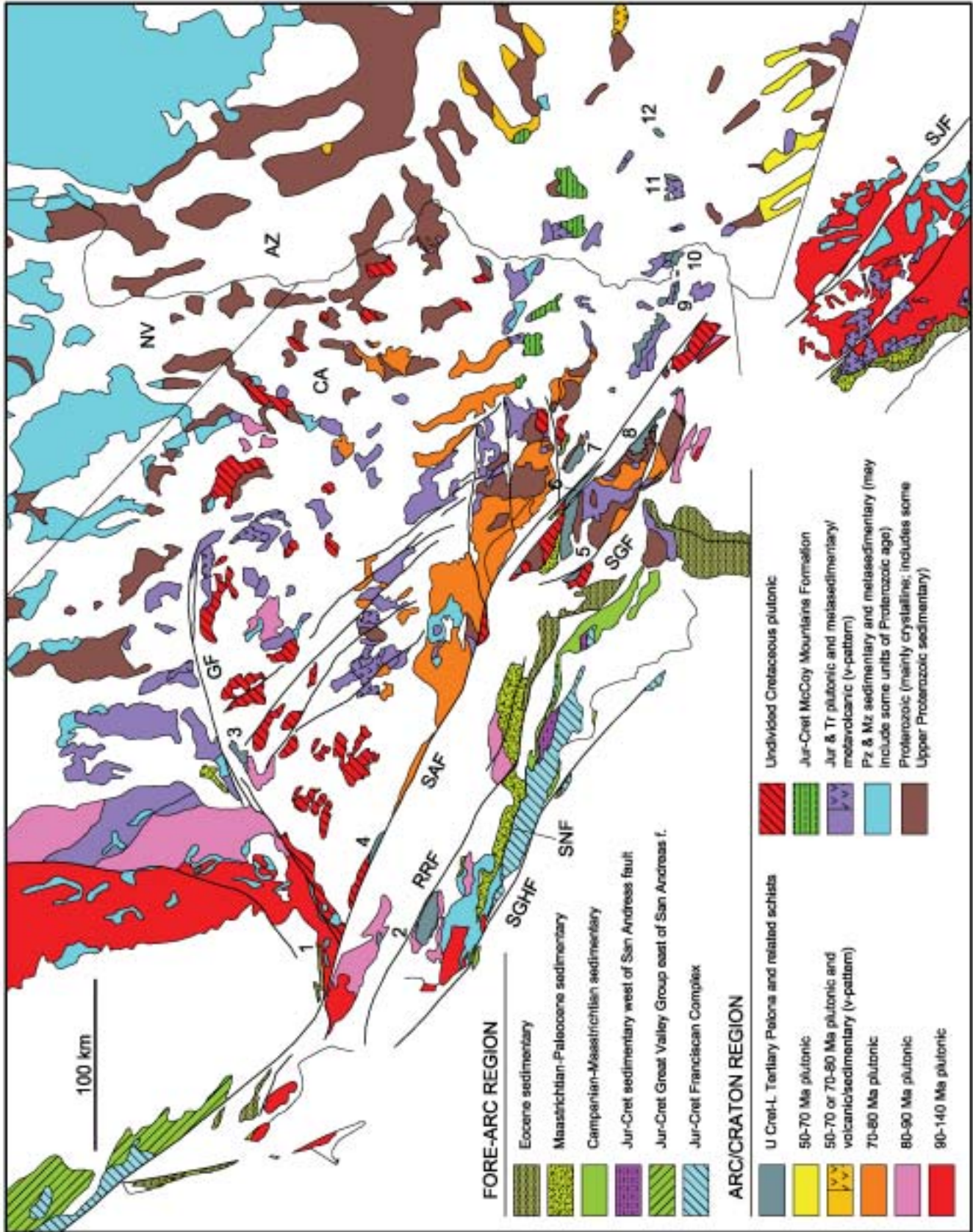
FORE-ARC REGION

- Eocene sedimentary
- Maastrichtian–Paleocene sedimentary
- Campanian–Maastrichtian sedimentary
- Jur–Cret sedimentary west of San Andreas fault
- Jur–Cret Great Valley Group east of San Andreas f.
- Jur–Cret Franciscan Complex

ARC/CRATON REGION

- U Cret–L. Tertiary Pelona and related schists
- 50–70 Ma plutonic
- 50–70 or 70–80 Ma plutonic and volcaniclastic/sedimentary (v-pattern)
- 70–80 Ma plutonic
- 80–90 Ma plutonic
- 90–140 Ma plutonic

- Undivided Cretaceous plutonic
- Jur–Cret McCoy Mountains Formation
- Jur & Tr plutonic and metasedimentary/ metavolcanic (v-pattern)
- Pz & Mz sedimentary and metasedimentary (may include some units of Proterozoic age)
- Proterozoic (mainly crystalline; includes some Upper Proterozoic sedimentary)

Figure 8. Pre–late Tertiary paleogeographic reconstruction of southern California, southwestern Arizona, and adjacent areas. Details regarding data sources employed in construction of this map are provided in Appendix 1. Abbreviations of fault names as in Figure 1.

strata within the northern portion of the Central California Coast Ranges. Crystallization ages of basement rocks of southeastern California and southwestern Arizona (Fig. 8) likewise mimic the detrital zircon U-Pb age systematics that we have measured for the Orocopia Schist from this area (Fig. 9; i.e., these schists contain high proportions of zircons yielding Proterozoic, Early Mesozoic, Late Cretaceous ages less than 80 Ma, and even earliest Tertiary ages; Jacobson et al., 2000). Maastrichtian to lower Eocene strata from southern Salinia and the Transverse Ranges contain detrital zircon suites similar to those from the southern schists (Fig. 8; Jacobson et al., 2002b).

Along-Strike Versus Across-Strike Control on Protolith Age and Provenance

Recognition of the northwest to southeast variation in age and provenance of the schist's protolith is one of the most conspicuous outcomes of this study. However, there is a significant ambiguity in interpreting the significance of this trend because the schist crops out along a relatively linear northwest-southeast array that transects the grain of the Mesozoic continental margin. Specifically, the Rand Schist and the schists of Portal Ridge and Sierra de Salinas tend to underlie older, more central to western parts of the Cretaceous arc (Fig. 8; Mattinson, 1978; Mattinson and James, 1985; Silver and Nourse, 1986; James and Mattinson, 1988; Pickett and Saleeby, 1993; Wood and Saleeby, 1997). In contrast, the Pelona and Orocopia Schists are located beneath the youngest (ca. 75 Ma), most inboard part of the main axis of voluminous Cretaceous magmatism (Sierra Pelona, San Gabriel Mountains, Orocopia Mountains; Fig. 8; Ehlig, 1981; Barth et al., 1995). In fact, the easternmost schist exposures in southwest Arizona are positioned east of the limit of extensive Cretaceous magmatism (Fig. 8; Powell, 1993; Tosdal et al., 1989; Haxel et al., 2002).

In light of this relationship, we cannot unambiguously determine the relative roles of position *along* versus *across* strike of the Late Cretaceous–early Tertiary continental margin in controlling detrital zircon age distributions and $^{40}Ar/^{39}Ar$ thermal histories (Fig. 7). Moreover, the highly schematic nature of Figure 8 (see Appendix 1) prevents us from determining the relative inboard-outboard or along-strike location of individual schist bodies on too fine a scale (e.g., the positions of the northern schists are not corrected for oroclinal bending of the southern Sierra Nevada). In any case, the above ambiguity must be kept in mind when considering the implications of our results for tectonic models to explain the genesis of the schists.

Evaluation of Models for Underplating of the Schists

Subduction Model

In the subduction model, graywacke supplied to the trench during the Late Cretaceous–earliest Tertiary was subducted and accreted to the base of the eroded continental lithosphere during shallow Laramide subduction of the Farallon slab (Fig. 2A; Crowell, 1968, 1981; Yeats, 1968; Burchfiel and Davis, 1981; Hamilton, 1987, 1988; Jacobson et al., 1996; Malin et al., 1995;

Wood and Saleeby, 1997). Such a model can explain the key observation of this study. Namely, erosion of basement source regions, trench deposition, underthrusting, accretion, and metamorphism are all predicted to occur in a very short time interval by the subduction model. Moreover, juxtaposition of Upper Cretaceous sediments and eugeoclinal lithologies is easily explained since these materials are expected to mix as they are subducted beneath the margin. Finally, because the model postulates that the lithosphere is eroded upwards to the base of the crust during low-angle Laramide subduction, any subsequently accreted trench sediments would have to post-date this erosion. Hence, the depositional age of the oldest accreted sediment in the subduction model can be no older than Late Cretaceous in age.

In its current form, the subduction model does not explicitly predict the systematic northwest to southeast younging of both protolith and metamorphic age that we observe in the schist (Fig. 7). We believe this pattern makes sense if it is primarily a function of distance normal to, rather than along strike of, the margin. This concept is illustrated in Figure 10 (Jacobson et al., 2002b). Before initiation of the Laramide orogeny, subduction of the Farallon slab at a moderate angle would have been associated with the "classic" belts of Franciscan Complex, Great Valley Group, and Sierran batholith (Fig. 10A). Beginning in the Late Cretaceous, gradual flattening of the subducting plate would result in progressive eastward removal of North American lower crust and mantle lithosphere and concomitant underplating of trench-derived graywacke. In the earliest stages of flat subduction (Fig. 10B), graywacke could be accreted only west of, and beneath, the medial Cretaceous arc. This material would be equivalent to the Rand Schist and schists of Portal Ridge and Sierra de Salinas. We postulate that equivalent age material was underplated to the south beneath the Peninsular Ranges. Post-intrusive rapid cooling initiated within the central and eastern Peninsular Ranges after 80 Ma support this hypothesis (George and Dokka, 1994; Grove et al., this volume, Chapter 13).

As the locus of tectonic erosion shifted inboard, graywacke precursors of the Pelona and Orocopia schists would have been accreted at positions that were ultimately farther east than the medial Cretaceous arc in southeastern California and southwestern Arizona (Fig. 10C). Also inherent in this model is that younger underplated material will have passed beneath previously accreted schist. The resultant thickening of the crust from below would have caused the older accreted material to be driven toward the surface, either by tectonic collapse at high structural levels (e.g., Platt, 1986) or by erosion (Yin, 2002). Thus, older schists accreted in the west are expected to have cooled through Ar closure while underplating continued to carry new material to the east. This provides a ready explanation for the parallel younging of detrital zircon and $^{40}Ar/^{39}Ar$ metamorphic cooling ages evident in Figure 7. It can also explain why cooling was more gradual in the southeast (i.e., larger gap between muscovite and biotite $^{40}Ar/^{39}Ar$ cooling ages). The southeasternmost schists would have been emplaced toward the end of Laramide low-angle subduction. Cessation of further underplating upon return
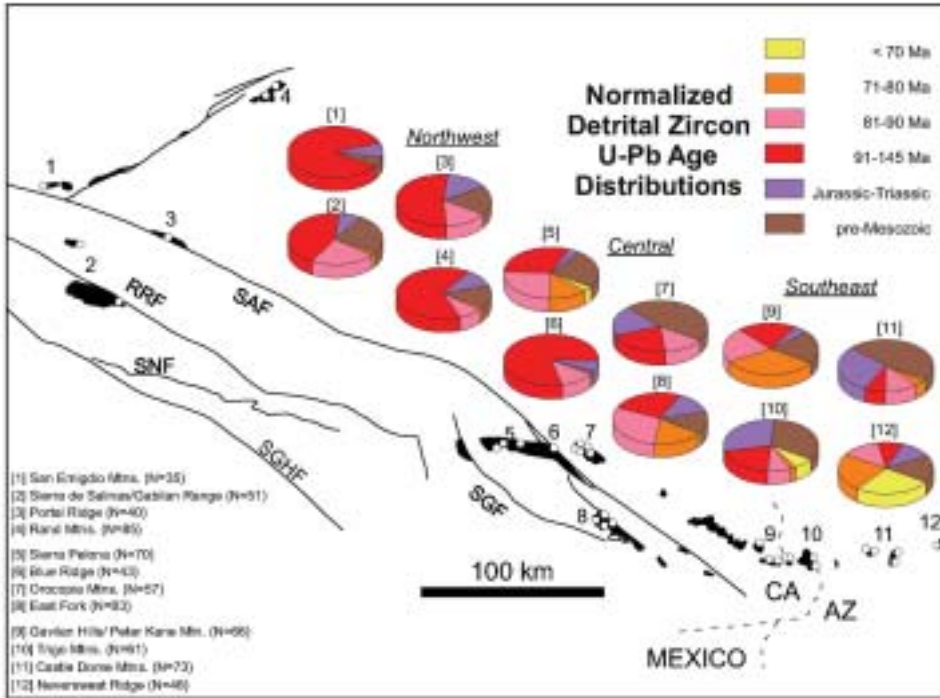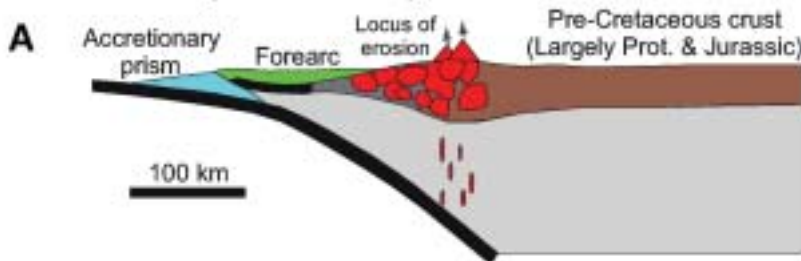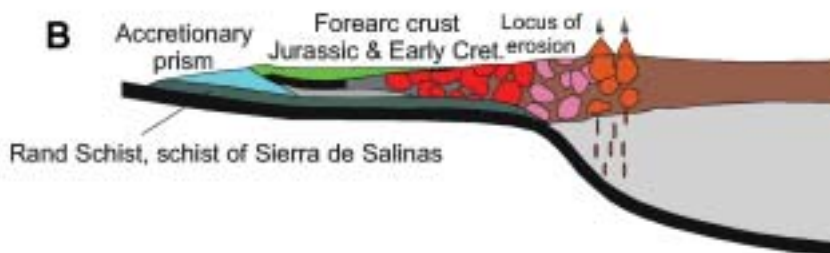
Figure 9. Normalized histograms illustrating northwest to southeast change in provenance for each of 12 major exposure areas of schist defined in Table 1. Age bins in histograms are the same as in Figure 6B–6D and correspond to age groupings used to subdivide crystalline rocks of equivalent age in Figure 8.
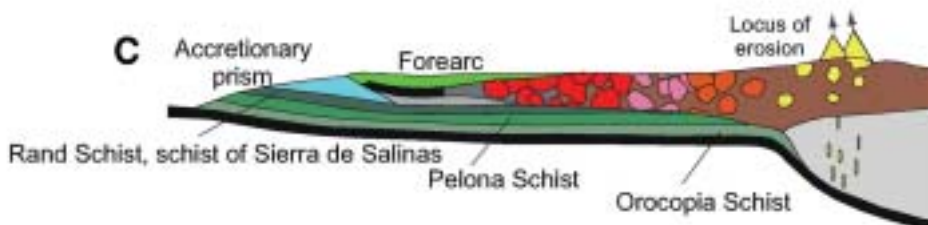

Figure 10. Tectonic model for underplating of schist. A: Before initiation of Laramide orogeny (i.e., subduction of Farallon slab proceeds at moderate angle). Beginning in Late Cretaceous, gradual flattening of subducting plate results in progressive eastward removal of North American lower crust and mantle lithosphere and concomitant underplating of trench-derived graywacke. B: In early stages of Laramide orogeny, graywacke is accreted west of, and beneath, medial Cretaceous arc (Rand Schist and schists of Portal Ridge and Sierra de Salinas). C: As locus of tectonic erosion shifted inboard, graywacke precursors of Pelona and Orocopia Schists are ultimately accreted east of medial Cretaceous arc in southeastern California and southwestern Arizona.

to a normal plate geometry would have removed the driving force for rapid exhumation.

The modified subduction model of Figure 10 may also help explain the northwest to southeast variation in provenance of the schist protolith. To some degree, this trend may simply reflect along-strike differences of bedrock geology; i.e., the dominance of middle to early Late Cretaceous intrusions in the Sierra Nevada compared to an abundance of Proterozoic, Jurassic, and latest Cretaceous crystalline rocks in the Mojave Desert and Transverse Ranges (Fig. 8). If continental drainages were orthogonal to the coast and there was little along-strike transport of sediment within the trench, then it is expected that northern (Rand-Portal Ridge-Sierra de Salinas) and southern (Pelona-Orocopia) schists would exhibit different sediment source characteristics. However, it is not clear that this process can explain the west to east variation in provenance exhibited just within the Pelona and Orocopia Schists (Fig. 9), which are restricted to a relatively small range of latitude. In this context, the model of Figure 10 predicts that sediment composition at any given point along the continental margin should evolve with time. This is consistent with previous studies of forearc sediments in central and southern California (Minch, 1979; Kies and Abbott, 1983; Linn et al., 1992; DeGraaff Surpless et al., 2002), which have suggested that drainage networks tapped progressively more easterly source areas as the magmatic front, the leading edge of the flat slab, and the region of underplating all shifted eastward during the Laramide orogeny (Fig. 10; Coney and Reynolds, 1977; Dickinson and Snyder, 1978; Bird, 1988). Because the Cretaceous arc is most voluminous in the west, the earliest sediment accreted (i.e., that represented by the Rand Schist and the schists of Portal Ridge and Sierra de Salinas) would have been dominated by this component. Sediment accreted during later stages of the Laramide orogeny would have been derived from more cratonal source regions farther east. As indicated in Figure 8, these would include mostly Proterozoic and Early Mesozoic arc detritus, with a smaller component of Laramide age (latest Cretaceous to early Tertiary) material. The net outcome is that the schist would appear to have a provenance that is broadly similar to the composition of the overlying crystalline rocks, exactly as we have observed.

Forearc Model

In this model (Fig. 2B), forearc strata are underthrust and accreted deep beneath the recently emplaced batholithic source region (Hall, 1991; Barth and Schneiderman, 1996; Saleeby, 1997). While the force driving this convergence is considered to be Laramide shallow subduction, underthrusting and metamorphism of the schist are considered to occur entirely within an intraplate setting. The forearc model is motivated to a large degree by the inferred difficulty of completely removing mantle lithosphere during shallow subduction. For example, low-angle subduction of the Nazca plate beneath northern Chile, which is commonly taken as an analog for the Laramide orogeny, has not resulted in substantial thinning of the South American mantle

lithosphere (Smalley and Isacks, 1987; Isacks, 1988; Allmendinger et al., 1990).

Previous discussion of the forearc model has focused upon the northwestern schist exposures (Rand Schist and the schists of Portal Ridge and Sierra de Salinas). The model provides a convenient explanation for the juxtaposition of Franciscan and arc rocks along the Sur–Nacimiento fault zone (Fig. 1; Hall, 1991; Barth and Schneiderman, 1996) and relationships involving exposure of deep crustal rocks in the southernmost Sierra Nevada (Saleeby, 1997). According to Barth and Schneiderman (1996), thrusting of the arc over the forearc was triggered by subduction of a buoyant oceanic plateau. In their view, the intersection between plateau and trench propagated from north to south, thus explaining the younging of the schist in that direction. Thus, the forearc model is sensible if the observed age progression among the schists (Fig. 7) is primarily a function of distance along strike of, rather than normal to, the margin.

It is clear that the forearc model can account for the short timescale for deposition and accretion observed for the northwestern schist exposures (Fig. 7). Moreover, Late Cretaceous strata are prominent in all of the forearc sequences depicted in Figure 8. The main difficulty we see with the model is that the youngest and generally more proximal parts of the forearc that are the most likely to have been overthrust are also the least likely to be spatially associated with eugeoclinal lithologies. Chert and basaltic rocks with mid-oceanic ridge compositional affinities constitute up to 10% of the schist (see Haxel et al., 1987, 2002; Dawson and Jacobson, 1989). These lithologies are most typically associated with distal Late Jurassic to Early Cretaceous forearc strata (Ingersoll, 1983, 1997) that we have not detected in our sampling of the schist. However, we cannot discount the possibility that other sources of eugeoclinal lithologies (such as the Sierran Foothills belt) were present along the western margin of the Cretaceous arc and were underthrust and mixed with forearc strata to produce the observed mix of rock types within the schist.

When the forearc model is extended to apply to all of the schist exposures, potential problems related to scale arise. For example, the schist bodies of southwestern Arizona lie on the cratonal side of the Cretaceous arc. If derived from the Great Valley Group, then the Arizona schists have been carried completely from one side of the arc to the other. This scale of intraplate thrusting (i.e., complete detachment of the arc) has not been recognized in the potentially analogous tectonic setting of low-angle subduction of the Nazca plate beneath northern Chile (Allmendinger et al., 1990).

Finally, the Andean example used to argue in favor of the forearc model may not be entirely relevant to areas proximal to the trench, i.e., the region where underplating of the schist would have occurred. This ambiguity is evident in the interpretation of Livaccari and Perry (1993) for the U.S. Cordillera. These authors argued, by analogy to the modern example from South America, that low-angle subduction during the Laramide orogeny did not result in *widespread* excision of North American lithosphere (e.g., beneath the Colorado Plateau and Rocky Mountains). Nonetheless, Livaccari and Perry (1993) specifically cited the

M. Grove et al.

Pelona and related schists as accretionary wedge deposits that indicated the removal of lowermost North American crust and underlying mantle lithosphere within several hundred kilometers of the trench.

Backarc Model

The backarc model is distinct from the subduction and forearc models in that it predicts that the schist's graywacke protolith was deposited not along the convergent margin but in a basin positioned behind the Cretaceous arc (Fig. 2D; Haxel and Dillon, 1978; Ehlig, 1981; Haxel et al., 2002). The model explicitly addresses the origin of the central and southeastern schist bodies. While originators of the model have not specified the age of the proposed rift basin, our results clearly require that it would have formed in the latest Cretaceous and/or earliest Tertiary. Hence, the possibility raised by Haxel and Tosdal (1986) that the backarc basin was somehow related to the Jurassic Mojave–Sonora Megashear of Silver and Anderson (1974) is precluded.

The principal prediction of the backarc model that is relevant to our study is the expectation that the provenance of basin-filling sediment should closely reflect the local basement (Haxel et al., 2002). Our results appear to uphold this prediction (see also Haxel et al., 2002). Specifically, the schist from the southeastern area contains high proportions of zircons yielding Proterozoic, Early Mesozoic, and Late Cretaceous ages <80 Ma, and even earliest Tertiary ages (Fig. 9) that strongly mimic the local basement geology (Fig. 8). It is somewhat unexpected that 14% of the zircons measured from the southeast group yield U-Pb ages that correspond to the emplacement interval (90–145 Ma) of the Early to early Late Cretaceous arc (Fig. 6). Grains of this age range occur in nearly all samples (Table 2). For the central group (Pelona Schist plus Orocopia Schist from the Orocopia Mountains), the proportion of 91–145 Ma zircons is even higher (38%). Inspection of Figure 8 reveals that the abundance of 91–145 Ma basement rocks from the Transverse Ranges, southeastern California, and southwestern Arizona is nowhere near the abundance implied by our detrital zircon results (particularly for the central schists). Nevertheless, recent characterization of the U-Pb age population of zircons from the McCoy Mountains Formation has clearly documented that 91–145 Ma arc detritus, of probable Sierran-Peninsular provenance, was supplied to basins in southeastern California (Barth et al., 2004). Hence, the existence of 91–145 Ma zircons from the southeastern schist cannot be considered unfavorable to the backarc model.

The main argument against the backarc model remains the lack of obvious evidence for either rift facies or a suture (see also Burchfiel and Davis, 1981; Crowell, 1981; Hamilton, 1987, 1988). These problems become monumental if the backarc model is applied to the northwestern schists. Haxel et al. (2002) acknowledge this and have argued that the origins of the northern and southern schists should be considered independently. However, despite the fact that the northern and southern schists differ in age, their similarities in rock types, geochemistry of the basalt protolith, structural style, and metamorphic petrology are so striking (Haxel et al., 1987; Jacobson et al., 1988; Dawson and Jacobson, 1989; Jacobson, 1995) that we find it difficult to accept that the different parts of the schist terrane could have been produced by such fundamentally dissimilar tectonic processes.

CONCLUSIONS

More than 850 ion microprobe U-Pb ages of detrital zircons from 40 schist metagraywacke samples that represent virtually all of the important exposures of the Pelona, Orocopia, and Rand Schists and the schists of Portal Ridge and Sierra de Salinas in southern California and southwestern Arizona indicate that the depositional age of their graywacke protolith is Late Cretaceous to earliest Tertiary (see also Jacobson et al., 2000; Barth et al., 2003a). Previous assessments that the schist's protolith was deposited prior to Late Jurassic or Early Cretaceous time appear to have been based upon interpretations of contact relationships that are no longer tenable.

Combined consideration of the youngest detrital zircon U-Pb ages and mica ^{40}Ar/^{39}Ar cooling ages indicate that the interval during which the schist's graywacke protolith was eroded from its source region, deposited, underthrust, accreted, and metamorphosed decreases systematically (in palinspastically restored coordinates) from about 92–90 Ma in the southwestern-most Sierra Nevada (San Emigdio mountains) to 55–40 Ma in the southwest Arizona (Neversweat Ridge). The average timescale for all these processes to have occurred is 13 ± 10 Ma and is locally too small (<~ 3 m.y.) to be resolved with the methods we have employed.

Two distinct source regions are indicated for the schists; the Rand Schist and schists of Portal Ridge and Sierra de Salinas were derived from material eroded from Early to early Late Cretaceous basement (like the Sierra Nevada batholith); the Orocopia Schist was derived from a heterogeneous assemblage of Proterozoic, Triassic, Jurassic, and latest Cretaceous to earliest Tertiary crystalline rocks (like basement in the Mojave/ Transverse Ranges/southwest Arizona/northern Sonora). The Pelona Schist is transitional between the two.

Our U-Pb detrital zircon and ^{40}Ar/^{39}Ar mica age results do not appear to permit us to exclude any of the models proposed for the origin of the schist. The backarc model appears untenable on the basis of independent evidence. We prefer the subduction model but recognize that the forearc model is also capable of explaining key aspects of our data set. Additional tests are required to select between the two.

APPENDIX 1: PALINSPASTIC RESTORATION OF SOUTHWEST NORTH AMERICA

To compare detrital zircon populations in the schist with potential source terranes, we developed a simplified palinspastic reconstruction of southern California and adjoining areas starting with a present-day geologic base compiled from a variety of sources. Primary references were Jennings (1977) and Powell (1993) for California, Richard et al. (2000) for Arizona, and Burchfiel et al. (1992) for Nevada. (Additional sources and a detailed listing of the sequence of steps utilized to generate the reconstruction can be obtained from the GSA Data Repository; see footnote 1.) An ideal palinspastic restoration for interpreting detrital zircon suites within the Pelona and related schists would take into account all compressional, extensional, translational, and rotational deformation since deposition of the schist protolith. Construction of such a map, however, is hindered by insufficient, ambiguous, and/or contradictory evidence regarding Cenozoic deformational history. Furthermore, geologic uncertainty is compounded by geometric complexities associated with drafting an accurate, balanced reconstruction for such a large area of inhomogeneous, multiphase deformation. Easiest, and what we concentrated on here, was to restore those strike-slip faults oriented sub-parallel to the continental margin (e.g., San Andreas, San Gabriel, San Jacinto, Punchbowl, San Gregorio-Hosgri, Rinconada-Reliz, etc.). Partitioning of slip among some of these faults is controversial (Powell, 1993; Dickinson, 1996). We followed Crowell (1962), Ehlig (1981), and Dillon and Ehlig (1993) in utilizing 240 km of displacement on the San Andreas fault and 60 km on the San Gabriel fault. Further discussion of this issue (including additional sources and a detailed listing of the sequence of steps utilized to generate the reconstruction) is presented in the GSA Data Repository (see footnote 1). We also utilized paleomagnetic data of Luyendyk et al. (1985; see also Dickinson, 1996) to back-rotate the western Transverse Ranges. The position of this region along the western edge of the map minimizes the problem of maintaining continuity between units. In contrast, we did not restore any east-west–trending left-lateral faults, such as the Garlock fault or those of the eastern Transverse Ranges. Balancing the complex gaps and overlaps that would result from removing the slip on these faults is beyond the scope of this study. For similar reasons, we did not correct for inferred rotations in the eastern Transverse Ranges or southern Sierra Nevada and Mojave Desert (Kanter and McWilliams, 1982; Luyendyk et al., 1985; Dokka and Ross, 1995). Nor did we take into account middle to late Tertiary extension, which affected the region from Death Valley southeastward to the corridor of the lower Colorado River (e.g., Davis

and Coney, 1979), despite the fact that extension has greatly altered the surface geology compared to Late Cretaceous–early Tertiary time. Notwithstanding these limitations, we consider that Figure 8 accurately portrays the *first-order* distribution of basement terranes within southern California and adjacent areas during the time of deposition of the schist protolith.

APPENDIX 2: SAMPLE LOCATION DETAILS

Sierra de Salinas and Gabilan Range

The Sierra de Salinas is underlain by one of the largest bodies of schist, yet it is not well studied because of poor exposure and lack of accessibility to private land. We include with the Sierra de Salinas body a smaller outcropping in the Gabilan Range to the northeast across the Rinconada-Reliz fault (Ross, 1976, 1984; James and Mattinson, 1988). We analyzed one sample from the Sierra de Salinas (DR-1656) and one from the Gabilan Range (JM80–102). Both were supplied by J.M. Mattinson of the University of California, Santa Barbara, with the sample from the Sierra de Salinas having originally been collected by D.C. Ross of the U.S. Geological Survey. We also incorporated U-Pb ion probe results from the three biotite schists of Barth et al. (2003a) from the Sierra de Salinas (02-242, 02-245, and 02-258) measured into our database. The schist of Sierra de Salinas is metamorphosed to the middle to upper amphibolite facies (Ross, 1976), which represents a higher peak temperature of metamorphism than was attained in most other bodies of the schist.

The schist bodies in the Sierra de Salinas and Gabilan Range are bordered by Cretaceous granitoid intrusions, some as young as 82 Ma (Barth et al., 2003a), although the contact relations have long been a matter of debate. Ross and Brabb (1973) and Ross (1974) interpreted the contacts as faults based on their straightness and the striking paucity of intrusions within the schists. Ross (1976), in contrast, concluded that the granitoids do intrude the schist along its margins, a view also taken by James and Mattinson (1988). However, detrital zircon ages for the schist demonstrate that the schist protolith is younger than the crystallization age of the adjacent pluton (see also Barth et al., 2003a). This, and the fact that the schists exhibit younger biotite $^{40}Ar/^{39}Ar$ ages than the plutons (70–71 Ma versus 75–76 Ma), requires that the contacts are faults.

Portal Ridge

The schist of Portal Ridge forms a sliver northeast of the San Andreas fault on the southwest edge of the Mojave Desert (Evans, 1966; Ross, 1976). This body likely correlates with the schist of Sierra de Salinas and shows similar high-grade metamorphism (middle to upper amphibolite facies). Nonetheless, we are impressed by the likeness in composition and proportion of rock types to the more typical parts of the schist. We analyzed one sample from this area (PR150).

San Emigdio Mountains

The Rand Schist in the San Emigdio Mountains is the most recently recognized of the schist bodies (James, 1986; James and Mattinson, 1988; Ross, 1989). It is not well exposed and has not received detailed study. Nonetheless, descriptions by the above workers and our own limited observations give us no reason to doubt that this body is correlative with the type Rand Schist. James (1986) and James and Mattinson (1988) concluded that the schist in this area was intruded after metamorphism by the 131 Ma tonalite of Antimony Peak. This implies an Early Cretaceous or older age for both the protolith and

M. Grove et al.

metamorphism. Ross (1989), however, mapped the contact between the schist and tonalite as a fault. Our one sample (99–57) was collected near the contact and exhibits a protomylonitic texture. Based on this deformational fabric, the fact that we observed no igneous intrusions within the schist, and our finding that detrital zircons in the schist are younger than the age of the tonalite, we concur with Ross (1989) that the contact is a fault.

Rand Mountains

The Rand Mountains comprise the type locality of the Rand Schist (Hulin, 1925; Silver et al., 1984; Silver and Nourse, 1986; Postlethwaite and Jacobson, 1987). Approximately 3 km of structural section is exposed in a post-metamorphic antiform. We analyzed one sample (RA169) from the structurally deepest, epidote-blueschist part of the section in the core of the antiform and one sample (RA170) belonging to the albite-epidote amphibolite facies from the top of the section in the southwestern part of the range. Total structural thickness in the area is about 3 km.

Sierra Pelona

The Sierra Pelona is the type locality of the Pelona Schist (Hershey, 1912; Harvill, 1969). Metamorphism ranges from greenschist to lower amphibolite facies and exhibits a clear inverted zonation (Graham and Powell, 1984). Our samples come from the middle (98–241, SP10) to lower (SP25D) parts of the section. Samples SP10 and SP25D were both collected adjacent to bodies of metabasite. The locality of SP25D is relatively well known because it is the only place in the entire schist terrane where relict pillow structure is evident in the metabasite (Haxel et al., 1987; Dawson and Jacobson, 1989). Absence of primary igneous structures elsewhere is presumably due to the intense deformation and recrystallization.

Blue Ridge (San Gabriel Mountains)

Pelona Schist in the Blue Ridge area of the San Gabriel Mountains occurs as a sliver between the Punchbowl and San Andreas faults. Although the Blue Ridge body currently sits immediately adjacent to Pelona Schist on the southwest side of the Punchbowl fault (East Fork body), this juxtaposition is thought to be coincidental. Most workers consider that the Blue Ridge body has been offset from the east end of the Sierra Pelona (Dibblee, 1967, 1968; Ehlig, 1968). One sample (98–240) was analyzed from this area and lies within the albite-epidote amphibolite facies.

East Fork (San Gabriel Mountains)

Pelona Schist exposed along the East Fork of the San Gabriel River was first studied by Ehlig (1958), who recognized most of the relations still considered key to understanding the schists. These include the fact that the schist originated in the lower plate of a major regional thrust fault, the presence of inverted metamorphism related to underthrusting, the relatively high-P/low-T style of metamorphism, and the eugeoclinal nature of the protolith and its likely Mesozoic age. The East Fork area continues to draw attention because it preserves a 1-km-thick zone of mylonite at the base of the upper plate that appears to be a remnant of the original underthrust (Ehlig, 1958, 1968, 1981; Jacobson, 1983a, 1983b, 1997). In most other areas, the contact between schist and upper plate appears to be an exhumation

structure. The East Fork area exposes a structural thickness of 3–4 km. Metamorphism ranges from lower greenschist facies at the base to uppermost greenschist facies at the contact with the upper plate. We analyzed four samples, two from near the top of the section (98–237, SG69), one from the middle (SG532), and one from the base (SG533). Sample SG69 was collected adjacent to metabasite. Sample 98–237 was collected near metachert, which, in turn, is usually associated with metabasite.

Orocopia Mountains

The Orocopia Mountains form the type locality of the Orocopia Schist. However, according to the pre–San Andreas fault reconstructions of Crowell (1962), Ehlig (1981), and Dillon and Ehlig (1993), the Orocopia Mountains formerly occupied a position adjacent to the Pelona Schist of Blue Ridge and the Sierra Pelona (Fig. 3). A different reconstruction is presented by Powell (1993) and Matti and Morton (1993), who place the Orocopia Mountains opposite the East Fork body of Pelona schist prior to offset on the San Andreas fault. In any case, the Orocopia Schist of the Orocopia Mountains is relatively far removed from the other bodies of Orocopia Schist we analyzed in southeasternmost California and southwestern Arizona (Fig. 3). Consequently, in pooling our results, we combined analyzes from the Orocopia Mountains with those from the Pelona Schist of the Sierra Pelona, Blue Ridge, and East Fork areas, rather than with those from the other bodies of Orocopia Schist.

Orocopia Schist in the Orocopia Mountains is exposed in a broad, northwest-trending post metamorphic arch (Crowell, 1975; Jacobson and Dawson, 1995; Robinson and Frost, 1996). Metamorphism is mostly in the albite-epidote amphibolite facies but locally reaches lowermost amphibolite facies. In the northwest Orocopia Mountains, we analyzed two samples from near the top of the section (OR77B, OR307; both associated with metabasalt) and five near the base (OR312A, OR113, OR314, OR337, and OR15A). In the southeastern Orocopia Mountains, we analyzed three albite-epidote amphibolite facies specimens (KE2-24-03-1, KE2-4-03-3, and KE1-27-02-1) that were supplied to us by Kristen Ebert.

Peter Kane Mountain and Gavilan Hills

These are two closely spaced bodies of Orocopia Schist that lie within the southernmost part of the Chocolate Mountains. The Peter Kane Mountain area is distinctive in that the lower part of the section is intruded by widespread porphyry dikes and granodiorite plutons of latest Oligocene to earliest Miocene age (Haxel, 1977; Miller and Morton, 1977; Uselding et al., 2001). Hornfels texture is characteristic of the schist in this part of the section. The uppermost schist, however, is typical of that in other areas. The one sample from the Peter Kane Mountain body comes from the top of the section.

The Gavilan Hills are underlain by a relatively small outcropping of schist with an exposed structural thickness of only about 300 m (Haxel, 1977; Oyarzabal et al., 1997; Jacobson et al., 2002a). Both samples from this area (UG1417A, UG1500) come from the lower part of the section and were metamorphosed in the lowermost amphibolite facies. Sample UG1500 is associated with metabasite. It is an atypical variety rich in spessartine garnet and transitional to metachert.

Trigo Mountains and Marcus Wash

This area comprises one body of Orocopia Schist divided approximately in two by the Colorado River. The northern half, in Arizona,

is part of the Trigo Mountains. The part south of the Colorado River in California will be referred to as the "Marcus Wash schist area." We also include in this grouping a small (1 × 2 km) outcropping of schist to the west of the Marcus Wash body located between Picacho Wash and White Wash (Haxel et al., 1985). The Trigo Mountains include a number of lenses of metabasite tens to hundreds of meters in length which Haxel et al. (2002) correlated with the 163 Ma metadiorite of the Chocolate Mountains (Mukasa et al., 1984) on the basis of field and petrographic character. None of the bodies in the Trigo Mountains have been dated, however. Nor have they been chemically analyzed to determine whether or not they show an arc geochemical signature as is the case for the metadiorite (Haxel et al., 1987, 2002). We analyzed detrital zircons for two samples from the Trigo Mountains (TR23, TR24A), both collected from metagraywacke immediately adjacent to the above mafic bodies. A third sample was analyzed from the Marcus Wash body (MW10) and yet another from the body between Picacho Wash and White Wash (YN17).

Castle Dome Mountains

The Castle Dome Mountains are important because of their position far inboard of the continental margin. Schist is exposed as separate bodies in the southwestern and southeastern parts of the range (Haxel et al., 2002). Appearance is identical to that of Orocopia Schist in ranges to the west; i.e., we are confident that these bodies should be included in the schist terrane. The schist in the southwest Castle Dome Mountains is heavily intruded by dikes and small stocks of early Miocene rhyolite porphyry. Two samples (CD7, CD9) were analyzed from this area. Schist in the southeastern part of the range is much less intruded than that in the southwest. Two samples (KE4 and KE6) were analyzed from the southeast. Cursory examination of both areas suggests metamorphism in the lowermost amphibolite facies.

Neversweat Ridge

Neversweat Ridge includes the easternmost outcrop of Orocopia Schist (Haxel et al., 2002). As is the case in the southwest Castle Dome Mountains, schist at Neversweat Ridge is strongly intruded by early Miocene rhyolite porphyry, and much of it is converted to hornfels or altered to chlorite and clay minerals (Haxel et al., 2002). Nonetheless, abundance of graphitic poikiloblasts of sodic plagioclase in metagraywacke and local presence of metachert and metabasite provide convincing evidence that this body is correlative with the type Orocopia Schist. Two samples, NR-1 and NR-2, were analyzed from this area.

APPENDIX 3: U-Pb Analytical Techniques

Zircon crystals were hand-selected from heavy mineral concentrates (ρ>3.30) obtained from the <250 μm size fraction. Grains were selected to be representative of the range of size, color, and morphology, with the exception that those with inclusions were avoided. Zircon grains mounted on double-sided tape were potted in epoxy, sectioned with 4000 grit SiC paper, and polished to 0.3 μm with polycrystalline diamond. Sample mounts were then ultrasonically cleaned and coated with Au. With the exception of Barth et al. (2003a) samples 02-342, 02-345, and 02-358, U-Pb ages were obtained using the University of California at Los Angeles Cameca ims 1270 ion microprobe (Dalrymple et al., 1999). A mass-filtered 10–20 nA $^{16}O^-$ beam with 22.5 kV impact energy was focused to a 30–35 μm spot. The region immediately above the sample surface was flooded with O_2 at a pressure of ~4 10^{-3} Pa. This has the effect of increasing Pb^+ yields by a factor of ~1.7. Secondary ions were extracted at 10 kV with an energy

band-pass of 50 eV. The mass spectrometer was tuned to obtain a mass resolution (~5000) that was sufficient to resolve the most troublesome molecular interferences (i.e., those adjacent to the Pb peaks). For most samples we took 15 cycles of measurements at $^{94}Zr_2^{16}O$, ^{204}Pb, ^{206}Pb, ^{207}Pb, ^{208}Pb, ^{232}Th, ^{238}U, and $^{238}U^{16}O$. Characteristics of the energy spectra of Th+, U+, and UO+ (relative to the other ions) lead us to apply small energy offsets so that these species could be measured at their maximum intensities.

For most samples we used ^{208}Pb as a proxy for common Pb (Compston et al., 1984). While this worked well for Th-poor samples, our initial analyses were forced to rely upon measurement of ^{204}Pb since ^{208}Pb and ^{232}Th were not determined (Jacobson et al., 2000). Nearly all of our samples yielded initially high common Pb signals derived from surficial contamination that rapidly decayed over the first several minutes of sputtering. Because of this behavior, we pre-sputtered the sample surface for about four minutes before taking measurements. During this interval, we performed ion imaging to align the analysis pit with the optical axis of the instrument and peak centering to fine-tune the mass calibration. Because sputtering proceeds more slowly at the edges of the crater than in the central region, resolvable surface contamination continued to contribute to the measured Pb signal after pre-sputtering had been completed. To further enhance the radiogenic lead yield, we cropped the ion beam with the field aperture to permit only ions sputtered from the central portion of the crater to be transmitted through the mass spectrometer.

The relative sensitivities for Pb and U were determined on reference zircon AS-3 (Paces and Miller, 1993) using a modified calibration technique described in Compston et al. (1984). Calibration data obtained from all of our standard measurements are displayed in Figure A1A and listed in Table A1. Assuming that analytical error alone is the main source of the observed variations, we estimate that the reproducibility of our $^{206}Pb/^{238}U$ apparent ages for such non-radiogenic samples is 3–5 % (Fig. A1B). This is reflected by the spread of $^{206}Pb/^{238}U$ determined for our AS-3 zircon standard data (Fig. A1C). More precise results (~2%) are anticipated for Proterozoic $^{207}Pb/^{206}Pb$ ages that are independent of the Pb-U relative sensitivity factor (Fig. A1D).

APPENDIX 4: $^{40}Ar/^{39}Ar$ Analytical Techniques

Hand-selected muscovite and biotite samples (~5 mg) were wrapped in copper foil and packed along with Fish Canyon sanidine flux monitors in quartz tubes that were evacuated and sealed. Sample results reported in this paper originated from three separate irradiations at the University of Michigan's Ford reactor (L67 position). In addition, several samples were irradiated in the McMaster Reactor (Ontario, Canada). See McDougall and Harrison (1999) for more information regarding these facilities and $^{40}Ar/^{39}Ar$ irradiation procedures. In all instances, ^{39}Ar production from ^{39}K (J-factor) was monitored with Fish Canyon sanidine (27.8 ± 0.3 Ma; Cebula et al., 1986) that had been interspersed with samples in each tube (1 cm spacing). Correction factors for nucleogenic K- and Ca-derived argon were determined by measuring K_2SO_4 and CaF_2 salts that were included with each irradiation. Because several irradiations were performed, it is inefficient to include further information here. Instead, we provide data reduction parameters relevant to each sample in the GSA Data Repository (see footnote 1). This information includes irradiation history and the date of $^{40}Ar/^{39}Ar$ analysis, all irradiation parameters (J, $^{40}Ar/^{39}Ar_K$, $^{38}Ar/^{39}Ar_K$, $^{36}Ar/^{37}Ar_{Ca}$, and $^{39}Ar/^{37}Ar_{Ca}$) instrumental backgrounds (m/e 40, 39,38,37,and 36), and mass discrimination (based upon blank-corrected measurement of atmospheric $^{40}Ar/^{36}Ar$).

Incremental heating was conducted with a double vacuum Ta furnace (details provided in Lovera et al., 1997). Temperature was generally increased from 500 to 1350 °C in 15-min intervals. Evolved gas was transferred by expansion and purified with an SAES ST-101 50 l/s
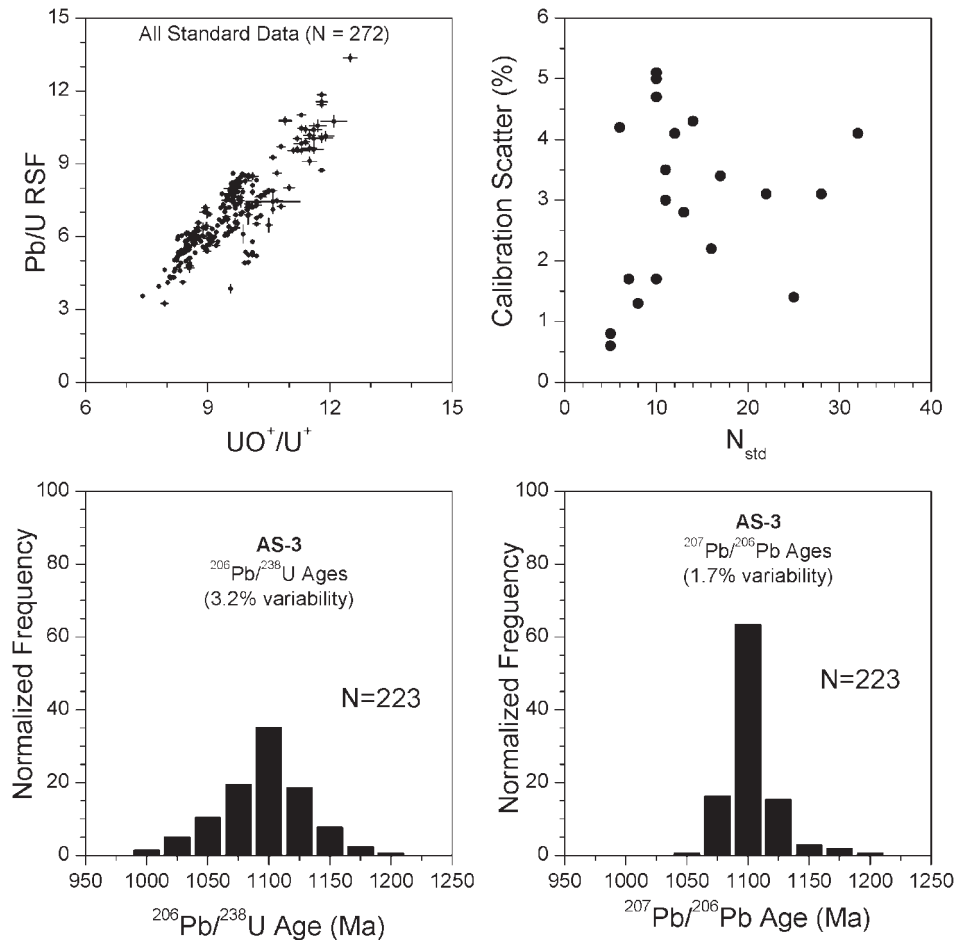
M. Grove et al.

Figure A1. Summary of U-Pb calibration data (see Appendix 3). A: Plot of Pb/U relative sensitivity factor (RSF) vs. UO^+/U^+ for determined from measurements of AS-3 standard zircon. B: Mean reproducibility of calibration array used to define U-Pb relative sensitivity factor is 3%. C: Histogram of $^{206}Pb/^{238}U$ ages calculated for AS-3 standard zircon. D: Histogram of $^{207}Pb/^{206}Pb$ ages calculated for AS-3 standard zircon.

getter pump in a LABVIEW automated, all-stainless steel extraction line. Note that values quoted for absolute quantities of ^{39}Ar have been normalized to 100% gas delivery to the mass spectrometer. Although 66% of the gas was generally transferred to the mass spectrometer, quantities of gas that exceeded the linear range of the detection system were split statically according to previously calibrated procedures. Argon isotopic measurements were performed using an automated VG1200S mass spectrometer equipped with a Baur-Signar ion source and an axially fitted electron multiplier (Quidelleur et al., 1997). The instrument is typically operated at an Ar sensitivity of 4×10^{-17} mol/mV. Apparent ages were calculated using conventional decay constants and isotopic abundances (Steiger and Jäger, 1977).

REFERENCES CITED

Allmendinger, R.W., Figueroa, D., Snyder, D., Beer, J., Mpodozis, C., and Isacks, B.L., 1990, Foreland shortening and crustal balancing in the Andes at 30°S latitude: Tectonics, v. 9, p. 789–809.

Armstrong, R.L., and Suppe, J., 1973, Potassium-argon geochronometry of Mesozoic igneous rocks in Nevada, Utah, and southern California: Geological Society of America Bulletin, v. 84, p. 1375–1392.

Barth, A.P., 1990, Mid-crustal emplacement of Mesozoic plutons, San Gabriel Mountains, California, and implications for the geologic history of the San Gabriel terrane: Geological Society of America Memoir 174, p. 33–45.

Barth, A.P., and Schneiderman, J.S., 1996, A comparison of structures in the Andean orogen of northern Chile and exhumed midcrustal structures in southern California, USA: An analogy in tectonic style: International Geology Review, v. 38, p. 1075–1085.

Barth, A.P., Wooden, J.L., Tosdal, R.M., and Morrison, J., 1995, Crustal contamination in the petrogenesis of a calc-alkalic rock series: Josephine Mountain intrusion, California: Geological Society of America Bulletin, v. 107, p. 201–211.

Barth, A.P., Wooden, J.L., Grove, M., Jacobson, C.E., and Dawson, J.P., 2003a, U-Pb zircon geochronology of rocks in the Salinas Valley region of California: A reevaluation of the crustal structure and origin of the Salinian Block: Geology, v. 31, p. 517–520.

Barth, A.P., Coleman, D.S., Grove, M., Jacobson, C.E., Miller, B.V., and Wooden, J.L., 2003b, Geochronology of the Randsburg Granodiorite: Reevaluation of the tectonics of the southern Sierra Nevada and western Mojave Desert: Geological Society of America Abstracts with Programs, v. 35, no. 4, p. 70.

Barth, A.P., Wooden, J.L., Jacobson, C.E., and Probst, K., 2004, U-Pb geochronology and geochemistry of the McCoy Mountains Formation, southeastern California: A Cretaceous retro-arc foreland basin: Geological Society of America Bulletin (in press).

Bender, E.E., Morrison, J., Anderson, J.L., and Wooden, J.L., 1993, Early Proterozoic ties between two suspect terranes and the Mojave crustal block of the southwestern U.S.: Journal of Geology, v. 101, p. 715–728.

Bird, P., 1988, Formation of the Rocky Mountains, western United States: A continuum computer model: Science, v. 239, p. 1501–1507.

Burchfiel, B.C., and Davis, G.A., 1981, Mojave Desert and environs, *in* Ernst, W.G., ed., The geotectonic development of California (Rubey Vol. I): Englewood Cliffs, New Jersey, Prentice Hall, p. 217–252.

Burchfiel, B.C., Cowan, D.S., and Davis, G.A., 1992, Tectonic overview of the Cordilleran orogen in the western United States, *in* Burchfiel, B.C.,

TABLE A1. SUMMARY OF U-Pb CALIBRATION DATA

Samples Analyzed	Session	Calibration*[†] scatter (%)	$UO^+/U^{+§}$ (Minimum)	$UO^+/U^{+§}$ (Maximum)	Slope[†]	Intercept[†]	N_{std}	N_{unk}
98-240	09/18/98	1.3	7.38	8.70	1.5	–7.3	8	26
UG1417A	11/13/98	1.7	9.53	10.00	2.3	–14.4	7	27
UG1417A	11/28/98	0.6	10.90	11.30	0.8	1.9	5	18
98-241	02/06/99	2.8	8.98	9.34	2.5	–16.8	13	23
98-241	04/02/99	4.2	8.70	9.00	2.5	–16.1	6	27
98-240	04/04/99	3.4	8.44	10.00	1.6	–8.4	17	21
PR150, RA170	08/26/99	1.4	7.93	8.85	1.8	–9.7	25	79
99-57, RA169	11/29/99	4.1	8.19	8.97	1.7	–8.2	32	61
98-237, SG533	03/23/00	4.7	11.30	12.30	2.0	–14.6	10	42
SG533	03/23/00	3.5	10.90	12.30	1.0	–1.7	11	21
CD7, NR2	03/25/00	5.1	11.40	12.10	2.5	–18.8	10	68
CD9, MW10, OR30, PK114B, YN17	07/25/00	3.0	9.35	9.78	2.5	–16.1	11	50
SG69, SG532, SP10, SP25D	07/26/00	3.1	9.32	9.91	2.5	–16.3	22	40
OR-77B, OR307, PK114B	07/27/00	3.1	9.32	9.91	2.5	–16.1	28	23
KE4, KE6, NR1	03/17/01	4.1	8.93	10.10	2.5	–16.2	12	30
JM80-102, NR1	03/18/01	4.3	8.46	10.10	2.4	–15.9	14	29
TR23, TR24C	03/19/01	5.0	9.13	9.86	2.3	–14.9	10	12
TR23, TR24C	04/01/01	1.7	9.25	9.85	2.4	–16.6	10	22
DR-1656, UG1500	06/11/01	2.2	9.21	10.50	1.9	–11.5	16	38
JM80-102	06/13/01	0.8	10.00	10.60	1.4	–6.3	5	5
OR312A, OR313	01/30/02	2.9	7.76	8.25	2.0	–11.4	9	19
99-57, OR314	02/03/02	3.3	9.28	9.74	2.0	–12.6	8	20

*Calibration scatter defined as 100 x [1 standard deviation of AS-3 standard measurements]/[mean $^{206}Pb/^{238}U$ age of AS-3 standard measurements].

[†]Pb-U relative sensitivity obtained from: RSF_{Pb-U} = slope x UO/U + intercept.

[§]Range of UO^+/U^+ values defined by the standard data.

Lipman, P.W., and Zoback, M.L., eds., The Cordilleran orogen: Conterminous U.S.: Boulder, Colorado, Geological Society of America, Geology of North America, v. G-3, p. 407–479.

Carson, C.J., Ague, J.J., Grove, M., Coath, C.D., and Harrison, T.M., 2002, U-Pb isotopic behavior of zircon during upper-amphibolite facies fluid infiltration in the Napier Complex, east Antarctica: Earth and Planetary Science Letters, v. 199, p. 287–310.

Cebula, G.T., Kunk, M.J., Mehnert, H.H., Naeser, C.W., Obradovich, J.D., and Sutter, J.F., 1986, The Fish Canyon Tuff, a potential standard for the $^{40}Ar/^{39}Ar$ and fission-track dating methods: TERRA Cognita, v. 6, p. 139–140.

Chen, J.H., and Moore, J.G., 1982, Uranium-lead isotopic ages from the Sierra Nevada batholith, California: Journal of Geophysical Research, v. 87, p. 4761–4784.

Cherniak, D.J., and Watson, E.B., 2000, Pb diffusion in zircon: Chemical Geology, v. 172, p. 5–24.

Compston, W., Williams, I.S., and Meyer, C.E., 1984, U-Pb geochronology of zircons from lunar breccia 73217 using a sensitive high mass-resolution ion microprobe: Journal of Geophysical Research B Supplement, v. 89, p. 525–534.

Coney, P.J., and Reynolds, S.J., 1977, Cordilleran Benioff zones: Nature, v. 270, p. 403–406.

Crowell, J.C., 1962, Displacement along the San Andreas fault, California: Boulder, Colorado, Geological Society of America Special Paper 71, 61 p.

Crowell, J.C., 1968, Movement histories of faults in the Transverse Ranges and speculations on the tectonic history of California, *in* Dickinson, W.R., and Grantz, A. eds., Proceedings of conference on geologic problems of San Andreas fault system: Stanford University Publications in the Geological Sciences, v. 11, p. 323–341.

Crowell, J.C., 1975, Geologic sketch of the Orocopia Mountains, southeastern California, *in* Crowell, J.C., ed., San Andreas fault in southern California: California Division of Mines and Geology Special Report 118, p. 99–110.

Crowell, J.C., 1981, An outline of the tectonic history of southeastern California, *in* Ernst, W.G., ed., The geotectonic development of California (Rubey Vol. I): Englewood Cliffs, New Jersey, Prentice Hall, p. 583–600.

Dalrymple, G.B., Grove, M., Lovera, O.M., Harrison, T.M., Hulen, J.B., and Lanphere, M.A., 1999, Age and thermal history of The Geysers plutonic complex (felsite unit), Geysers geothermal field, California: A $^{40}Ar/^{39}Ar$ and U-Pb study: Earth and Planetary Science Letters, v. 173, p. 285–298.

Davis, G.H., and Coney, P.J., 1979, Geologic development of the Cordilleran metamorphic core complexes: Geology, v. 7, p. 120–124.

Dawson, M.R., and Jacobson, C.E., 1989, Geochemistry and origin of mafic rocks from the Pelona, Orocopia, and Rand Schists, southern California: Earth and Planetary Science Letters, v. 92, p. 371–385.

DeGraaff Surpless, K., Graham, S.A., Wooden, J.L., and McWilliams, M.O., 2002, Detrital zircon provenance analysis of the Great Valley Group,

California: Evolution of an arc-forearc system: Geological Society of America Bulletin, v. 114, p. 1564–1580.

Dibblee, T.W., Jr., 1967, Areal geology of the western Mojave Desert, California: U.S. Geological Survey Professional Paper 522, 153 p.

Dibblee, T.W., Jr., 1968, Displacements on the San Andreas fault system in the San Gabriel, San Bernardino, and San Jacinto Mountains, southern California, *in* Dickinson, W.R., and Grantz, A., eds., Proceedings of Conference on Geologic Problems of San Andreas Fault System: Stanford, California, Stanford University Publications in the Geological Sciences, v. 11, p. 260–278.

Dickinson, W.R., 1996, Kinematics of transrotational tectonism in the California Transverse Ranges and its contribution to cumulative slip along the San Andreas transform fault system: Boulder, Colorado, Geological Society of America Special Paper 305, 46 p.

Dickinson, W.R., and Snyder, W.S., 1978, Plate tectonics of the Laramide orogeny, *in* Matthews, V., III, ed., Laramide folding associated with basement block faulting in the western United States: Boulder, Colorado, Geological Society of America Memoir 151, p. 355–366.

Dickinson, W.R., Hopson, C.A., and Saleeby, J.B., 1996, Alternate origins of the Coast Range Ophiolite (California): Introduction and implications: GSA Today, v. 6, no. 2, p. 1–10.

Dillon, J.T., 1976, Geology of the Chocolate and Cargo Muchacho Mountains, southeasternmost California, California [Ph.D. thesis]: Santa Barbara, University of California, 405 p.

Dillon, J.T., and Ehlig, P.L., 1993, Displacement on the southern San Andreas fault, *in* Powell, R.E., Weldon, R.J., II, and Matti, J.C., eds., The San Andreas fault system: Displacement, palinspastic reconstruction, and geologic evolution: Boulder, Colorado, Geological Society of America Memoir 178, p. 199–216.

Dillon, J.T., Haxel, G.B., and Tosdal, R.M., 1990, Structural evidence for northeastward movement on the Chocolate Mountains thrust, southeasternmost California: Journal of Geophysical Research, v. 95, p. 19953–19971.

Dodson, M.H., Compston, W., Williams, I.S., and Wilson, J.F., 1988, A search for ancient detrital zircons in Zimbabwean sediments: Journal of the Geological Society [London], v. 145, p. 977–983.

Dokka, R.K., and Ross, T.M., 1995, Collapse of southwestern North America and the evolution of early Miocene detachment faults, metamorphic core complexes, the Sierra Nevada orocline, and the San Andreas fault system: Geology, v. 23, p. 1075–1078.

Drobeck, P.A., Hillemeyer, F.L., Frost, E.G., and Liebler, G.S., 1986, The Picacho mine: A gold mineralized detachment in southeastern California, *in* Beatty, B., and Wilkinson, P.A.K., eds., Frontiers in geology and ore deposits of Arizona and the southwest: Arizona Geological Society Digest, v. 16, p. 187–221.

Ehlig, P.L., 1958, The geology of the Mount Baldy region of the San Gabriel Mountains, California, California [Ph.D. thesis]: Los Angeles, University of California, 195 p.

Ehlig, P.L., 1968, Causes of distribution of Pelona, Rand, and Orocopia Schists along the San Andreas and Garlock faults, *in* Dickinson, W.R., and Grantz, A., eds., Proceedings of Conference on Geologic Problems of San Andreas Fault System: Stanford University Publications in the Geological Sciences, v. 11, p. 294–306.

Ehlig, P.L., 1981, Origin and tectonic history of the basement terrane of the San Gabriel Mountains, central Transverse Ranges, *in* Ernst, W.G., ed., The geotectonic development of California (Rubey Volume I): Englewood Cliffs, New Jersey, Prentice Hall, p. 253–283.

Evans, J.G., 1966, Structural analysis and movements of the San Andreas fault zone near Palmdale, southern California [Ph.D. thesis]: Los Angeles, University of California, 186 p.

Froude, D.O., Ireland, T.R., Kinny, P.D., Williams, I.S., Compston, W., Williams, I.R., and Myers, J.S., 1983, Ion microprobe identification of 4,100–4,200-Myr-old terrestrial zircons: Nature, v. 304, p. 616–618.

Geisler, T., Ulonska, M., Schleicher, H., Pidgeon, R.T., and van Bronswijk, W., 2001, Leaching and differential recrystallization of metamict zircon under experimental hydrothermal conditions: Contributions to Mineralogy and Petrology, v. 141, p. 53–65.

George, P.G., and Dokka, R.K., 1994, Major Late Cretaceous cooling events in the eastern Peninsular Ranges, California, and their implications for Cordilleran tectonics: Geological Society of America Bulletin, v. 106, p. 903–914.

Graham, C.M., and England, P.C., 1976, Thermal regimes and regional metamorphism in the vicinity of overthrust faults: An example of shear heating and inverted metamorphic zonation from southern California: Earth and Planetary Science Letters, v. 31, p. 142–152.

Graham, C.M., and Powell, R., 1984, A garnet-hornblende geothermometer: Calibration, testing, and application to the Pelona Schist, southern California: Journal of Metamorphic Geology, v. 2, p. 13–31.

Grove, M., and Bebout, G.E., 1995, Cretaceous tectonic evolution of coastal southern California: Insights from the Catalina Schist: Tectonics, v.14, p.1290–1308.

Grubensky, M.J., and Bagby, W.C., 1990, Miocene calc-alkaline magmatism, calderas, and crustal evolution in the Kofa and Castle Dome Mountains, southwestern Arizona: Journal of Geophysical Research, v. 95, p. 19989–20003.

Hall, C.A., Jr., 1991, Geology of the Point Sur-Lopez Point region, Coast Ranges, California: A part of the southern California allochthon: Boulder, Colorado, Geological Society of America Special Paper 266, 40 p.

Hamilton, W., 1987, Mesozoic geology and tectonics of the Big Maria Mountains region, southeastern California, *in* Dickinson, W.R., and Klute, M.A., eds., Mesozoic rocks of southern Arizona and adjacent areas: Arizona Geological Society Digest, v. 18, p. 33–47.

Hamilton, W., 1988, Tectonic setting and variations with depth of some Cretaceous and Cenozoic structural and magmatic systems of the western United States, *in* Ernst, W.G., ed., Metamorphism and crustal evolution of the western United States (Rubey Vol. VII): Englewood Cliffs, New Jersey, Prentice Hall, p. 1–40.

Harrison, T.M., Yin, A., Grove, M., Lovera, O.M., and Ryerson, F.J., 2000, The Zedong Window: A record of superposed Tertiary convergence in southeastern Tibet: Journal of Geophysical Research, v. 105, p. 19211–19230.

Harvill, L.L., 1969, Deformational history of the Pelona Schist, northwestern Los Angeles County, California [Ph.D. thesis]: Los Angeles, University of California, 117 p.

Haxel, G.B., 1977, The Orocopia Schist and the Chocolate Mountain Thrust, Picacho-Peter Kane mountain area, southeasternmost California [Ph.D. thesis]: Santa Barbara, University of California, 277 p.

Haxel, G.B., and Dillon, J.T., 1978, The Pelona-Orocopia Schist and Vincent–Chocolate Mountain thrust system, southern California, *in* Howell, D.G., and McDougall, K.A., eds., Mesozoic paleogeography of the western United States: Los Angeles, Society of Economic Paleontologists and Mineralogists Pacific Section Pacific Coast Paleogeography Symposium 2, p. 453–469.

Haxel, G.B., and Tosdal, R.M., 1986, Significance of the Orocopia Schist and Chocolate Mountains thrust in the late Mesozoic tectonic evolution of the southeastern California-southwestern Arizona region, *in* Beatty, B., and Wilkinson, P.A.K., eds., Frontiers in geology and ore deposits of Arizona and the Southwest: Arizona Geological Society Digest, v. 16, p. 52–61.

Haxel, G.B., Tosdal, R.M., and Dillon, J.T., 1985, Tectonic setting and lithology of the Winterhaven Formation: A new Mesozoic stratigraphic unit in southeasternmost California and southwestern Arizona: U.S. Geological Survey Bulletin 1599, 19 p.

Haxel, G.B., Budahn, J.R., Fries, T.L., King, B.W., White, L.D., and Aruscavage, P.J., 1987, Geochemistry of the Orocopia Schist, southeastern California: Summary, *in* Dickinson, W.R., and Klute, M.A., eds., Mesozoic rocks of southern Arizona and adjacent areas: Arizona Geological Society Digest, v. 18, p. 49–64.

Haxel, G.B, Jacobson, C.E., Richard, S.M., Tosdal, R.M., and Grubensky, M.J., 2002, The Orocopia Schist in southwest Arizona: Early Tertiary oceanic rocks trapped or transported far inland, *in* Barth, A.P., ed., Contributions to crustal evolution of the southwestern United States: Boulder, Colorado, Geological Society of America Special Paper 365, p. 99–128.

Hershey, O.H., 1912, The Belt and Pelona series: American Journal of Science, v. 34, p. 263–273.

Högdahl, K., Gromet, L.P., and Broman, C., 2001, Low P-T Caledonian resetting of U-rich Paleoproterozoic zircons, central Sweden: American Mineralogist, v. 86, p. 534–546.

Hulin, C.D., 1925, Geology and ore deposits of the Randsburg quadrangle, California: California State Mining Bureau Bulletin 95, 152 p.

Ingersoll, R.V., 1983, Petrofacies and provenance of Late Mesozoic forearc basin, northern and central California: American Association of Petroleum Geologists Bulletin, v. 67, p. 1125–1142.

Ingersoll, R.V., 1997, Phanerozoic tectonic evolution of central California and environs: International Geology Review, v. 39, p. 957–972.

Ireland, T.R., 1992, Crustal evolution of New Zealand—Evidence from age distributions of detrital zircons in western province paragneisses and Torlesse greywacke: Geochimica et Cosmochimica Acta, v. 56, p. 911–920.

Isacks, B.L., 1988, Uplift of the central Andean plateau and bending of the Bolivian orocline: Journal of Geophysical Research, v. 93, p. 3211–3231.

Jacobson, C.E., 1983a, Structural geology of the Pelona Schist and Vincent thrust, San Gabriel Mountains, California: Geological Society of America Bulletin, v. 94, p. 753–767.

Jacobson, C.E., 1983b, Relationship of deformation and metamorphism of the Pelona Schist to movement on the Vincent thrust, San Gabriel Mountains, southern California: American Journal of Science, v. 283, p. 587–604.

Jacobson, C.E., 1990, The ^{40}Ar/^{39}Ar geochronology of the Pelona Schist and related rocks, southern California: Journal of Geophysical Research, v. 95, p. 509–528.

Jacobson, C.E., 1995, Qualitative thermobarometry of inverted metamorphism in the Pelona and Rand Schists, southern California using calciferous amphibole in mafic schist: Journal of Metamorphic Geology, v. 13, p. 79–92.

Jacobson, C.E., 1997, Metamorphic convergence of the upper and lower plates of the Vincent thrust, San Gabriel Mountains, southern California: Journal of Metamorphic Geology, v. 15, p. 155–165.

Jacobson, C.E., and Dawson, M.R., 1995, Structural and metamorphic evolution of the Orocopia Schist and related rocks, southern California: Evidence for late movement on the Orocopia fault: Tectonics, v. 14, p. 933–944.

Jacobson, C.E., Dawson, M.R., and Postlethwaite, C.E., 1988, Structure, metamorphism, and tectonic significance of the Pelona, Orocopia, and Rand Schists, southern California, *in* Ernst, W.G., ed., Metamorphism and crustal evolution of the western United States (Rubey Vol. VII): Englewood Cliffs, New Jersey, Prentice Hall, p. 976–997.

Jacobson, C.E., Oyarzabal, F.R., and Haxel, G.B., 1996, Subduction and exhumation of the Pelona-Orocopia-Rand schists, southern California: Geology, v. 24, p. 547–550.

Jacobson, C.E., Barth, A.P., and Grove, M., 2000, Late Cretaceous protolith age and provenance of the Pelona and Orocopia Schists, southern California: Implications for evolution of the Cordilleran margin: Geology, v. 28, p. 219–222.

Jacobson, C.E., Grove, M., Stamp, M.M., Vucic, A., Oyarzabal, F.R., Haxel, G.B., Tosdal, R.M., and Sherrod, D.R., 2002a, Exhumation history of the Orocopia Schist and related rocks in the Gavilan Hills area of southeasternmost California, *in* Barth, A.P., ed., Contributions to crustal evolution of the southwestern United States: Boulder, Colorado, Geological Society of America Special Paper 365, p. 129–154.

Jacobson, C.E., Grove, M., Barth, A.P., Pedrick, J.N., and Vucic, A., 2002b, "Salmon tectonics" as a possible explanation for Laramide sedimentation and underplating of schist in southern California and southwestern Arizona: Geological Society of America Abstracts with Programs, v. 34, no. 6, p. 510.

James, E.W., 1986, U/Pb age of the Antimony Peak tonalite and its relation to Rand Schist in the San Emigdio Mountains, California: Geological Society of America Abstracts with Programs, v. 18, no. 2, p. 121.

James, E.W., and Mattinson, J.M., 1988, Metamorphic history of the Salinian block: An isotopic reconnaissance, *in* Ernst, W.G., ed., Metamorphism and crustal evolution of the western United States (Rubey Vol. VII): Englewood Cliffs, New Jersey, Prentice Hall, p. 938–952.

Jennings, C.W., compiler, 1977, Geologic map of California: California Division of Mines and Geology, scale 1:750,000, 1 sheet.

Kanter, L.R., and McWilliams, M.O., 1982, Rotation of the southernmost Sierra Nevada, California: Journal of Geophysical Research, v. 87, p. 3819–3830.

Kies, R.P., and Abbott, P.L., 1983, Rhyolite clast populations and tectonics in the California continental borderland: Journal of Sedimentary Petrology, v. 53, p. 461–475.

Kistler, R.W., and Champion, D.E., 2001, Rb-Sr whole-rock and mineral ages, K-Ar, ^{40}Ar/^{39}Ar, and U-Pb mineral ages, and Strontium, Lead, Neodymium, and Oxygen isotopic compositions for granitic rocks from the Salinian composite terrane, California: U.S. Geological Survey Open File Report 01-453, 84 p.

Kistler, R.W., and Peterman, Z.E., 1978, Reconstruction of crustal blocks in California on the basis of initial strontium isotopic compositions of Mesozoic granitic rocks: U.S. Geological Survey Professional Paper 1071, 17 p.

Kröner, A., Jaeckel, P., and Williams, I.S., 1994, Pb-loss patterns in zircons from a high-grade metamorphic terrain as revealed by different dating methods: U–Pb and Pb–Pb ages for igneous and metamorphic zircons from northern Sri Lanka: Precambrian Research, v. 66, p. 151–181.

Lee, J.K.W., Williams, I.S., and Ellis, D.J., 1997, Pb, U and Th diffusion in natural zircon: Nature, v. 390, p. 159–161.

Linn, A.M., DePaolo, D.J., and Ingersoll, R.V., 1992, Nd-Sr isotopic, geochemical, and petrographic stratigraphy and paleotectonic analysis: Mesozoic Great Valley forearc sedimentary rocks of California: Geological Society of America Bulletin, v. 104, p. 1264–1279.

Livaccari, R.F., and Perry, F.V., 1993, Isotopic evidence for preservation of Cordilleran lithospheric mantle during the Sevier-Laramide orogeny, Western United States: Geology, v. 21, p. 719–722.

Lovera, O.M., Grove, M., Harrison, T.M., and Mahon, K.I., 1997, Systematic analysis of K-feldspar ^{40}Ar/^{39}Ar step-heating experiments I: Significance of activation energy determinations: Geochimica et Cosmochimica Acta, v. 61, p. 3171–3192.

Luyendyk, B.P., Kamerling, M.J., Terres, R.R., and Hornafius, J.S., 1985, Simple shear of southern California during Neogene time suggested by paleomagnetic declinations: Journal of Geophysical Research, v. 90, p. 12454–12466.

Maas, R., Kinny, P.D., Williams, I.S., Froude, D.O., and Compston, W., 1992, The earth's oldest known crust—A geochronological and geochemical study of 3900–4200 Ma old detrital zircons from Mt. Narryer and Jack Hills, Western Australia: Geochimica et Cosmochimica Acta, v. 56, p. 1281–1300.

MacPherson, G.J., Phipps, S.P., and Grossman, J.N., 1990, Diverse sources for igneous blocks in Franciscan mélanges, California Coast Ranges: Journal of Geology, v. 98, p. 845–862.

Malin, P.E., Goodman, E.D., Henyey, T.L., Li, Y.G., Okaya, D.A., and Saleeby, J.B., 1995, Significance of seismic reflections beneath a tilted exposure of deep continental crust, Tehachapi Mountains, California: Journal of Geophysical Research, v. 100, p. 2069–2087.

Matti, J.C., and Morton, D.M., 1993, Paleogeographic evolution of the San Andreas fault in southern California: A reconstruction based on a new cross-fault correlation, *in* Powell, R.E., Weldon, R.J., and Matti, J.C., eds., The San Andreas fault system: Displacement, palinspastic reconstruction and geologic evolution: Boulder, Colorado, Geological Society of America Memoir 178, p. 107–159.

Mattinson, J.M., 1978, Age, origin, and thermal histories of some plutonic rocks from the Salinian block of California: Contributions to Mineralogy and Petrology, v. 67, p. 233–245.

Mattinson, J.M., 1990, Petrogenesis and evolution of the Salinian magmatic arc, *in* Anderson, J.L., ed., The nature and origin of Cordilleran magmatism: Boulder, Colorado, Geological Society of America Memoir 174, p. 237–250.

Mattinson, J.M., and James, E.W., 1985, Salinian block U/Pb age and isotopic variations: Implications for origin and emplacement of the Salinian terrane, *in* Howell, D.G., ed., Tectonostratigraphic terranes of the circum-Pacific region: Houston, Texas, Circum-Pacific Council for Energy and Mineral Resources Earth Science Series, no. 1, p. 215–226.

McDougall, I., and Harrison, T.M., 1999, Geochronology and thermochronology by the ^{40}Ar/^{39}Ar method, second edition: New York, Oxford University Press, 269 p.

Mezger, K., and Krogstad, E.J., 1997, Interpretation of discordant U-Pb zircon ages: An evaluation: Journal of Metamorphic Geology, v. 15, p. 127–140.

Miller, F.K., and Morton, D.M., 1977, Comparison of granitic intrusions in the Pelona and Orocopia Schists, southern California: U.S. Geological Survey Journal of Research, v. 5, p. 643–649.

Miller, J.S., Glazner, A.F., and Crowe, D.E., 1996, Muscovite-garnet granites in the Mojave Desert: Relation to crustal structure of the Cretaceous arc: Geology, v. 24, p. 335–338.

Miller, C.F., Hatcher, R.D., Harrison, T.M., Coath, C.D., and Gorisch, E.B., 1998, Cryptic crustal events elucidated through zone imaging and ion microprobe studies of zircon, southern Appalachian Blue-Ridge, North Carolina-Georgia: Geology, v. 26, p. 419–422.

Minch, J.A., 1979, The late-Mesozoic–early Tertiary framework of continental sedimentation, northern Peninsular Ranges, Baja California, Mexico, *in* Abbott, P.L., ed., Eocene depositional systems, San Diego: San Diego, Pacific Section, Society of Economic Paleontologists and Mineralogists, p. 43–68.

Mojzsis, S.J., and Harrison, T.M., 2002, Establishment of a 3.83-Ga magmatic age for the Akilia tonalite (southern West Greenland): Earth and Planetary Science Letters, v. 202, p. 563–576.

Mukasa, S.B., Dillon, J.T., and Tosdal, R.M., 1984, A Late Jurassic minimum age for the Pelona-Orocopia Schist protolith, southern California: Geological Society of America Abstracts with Programs, v. 16, p. 323.

Oyarzabal, F.R., Jacobson, C.E., and Haxel, G.B., 1997, Extensional reactivation of the Chocolate Mountains subduction thrust in the Gavilan Hills of southeastern California: Tectonics, v. 16, p. 650–661.

Paces, J.B., and Miller, J.D., 1993, Precise U-Pb age of Duluth Complex and related mafic intrusions, northeastern Minnesota: Geochronological insights into physical, petrogenetic, paleomagnetic, and tectonomagmatic

M. Grove et al.

processes associated with the 1.1 Ga midcontinent rift system: Journal of Geophysical Research, v. 98, p. 13997–14013.

Pickett, D.A., and Saleeby, J.B, 1993, Thermobarometric constraints on the depth of exposure and conditions of plutonism and metamorphism at deep levels of the Sierra Nevada batholith, Tehachapi Mountains, California: Journal of Geophysical Research, v. 98, p. 609–629.

Pidgeon, R.T., O'Neil, J.R., and Silver, L.T., 1966, Uranium and lead isotopic stability in a metamict zircon under experimental hydrothermal conditions: Science, v. 154, p. 1538–1540.

Platt, J.P., 1986, Dynamics of orogenic wedges and the uplift of high-pressure metamorphic rocks: Geological Society of America Bulletin, v. 97, p. 1037–1053.

Postlethwaite, C.E., and Jacobson, C.E., 1987, Early history and reactivation of the Rand thrust, southern California: Journal of Structural Geology, v. 9, p. 195–205.

Powell, R.E., 1993, Balanced palinspastic reconstruction of pre-late Cenozoic paleogeology, southern California, *in* Powell, R.E., Weldon, R.J., and Matti, J.C., eds., The San Andreas fault system: Displacement, palinspastic reconstruction, and geologic evolution: Boulder, Colorado, Geological Society of America Memoir 178, p. 1–106.

Quidelleur, X., Grove, M., Lovera, O.M., Harrison, T.M., Yin, A., and Ryerson, F.J., 1997, The thermal evolution and slip history of the Renbu Zedong thrust, southeastern Tibet: Journal of Geophysical Research, v. 102, p. 2659–2679.

Reynolds, S.J., 1988, Geologic map of Arizona: Arizona Geological Survey Map 26, scale 1:1,000,000, 1 sheet.

Richard, S.M., 1993, Palinspastic reconstruction of southeastern California and southwestern Arizona for the middle Miocene: Tectonics, v. 12, p. 830–854.

Richard, S.M., Reynolds, S.J., Spencer, J.E., and Pearthree, P.A., 2000, compilers, Geologic Map of Arizona: Arizona Geological Survey Map 35, scale 1:1,000,000, 1 sheet.

Robinson, K.L., and Frost, E.G., 1996, Orocopia Mountains detachment system: Progressive development of a tilted crustal slab and a half-graben sedimentary basin during regional extension, *in* Abbott, P.L., and Cooper, J.D., eds., American Association of Petroleum Geologists Field Conference Guide 73: Bakersfield, California, Pacific Section American Association of Petroleum Geologists, p. 277–284.

Ross, D.C., 1974, Map showing basement geology and location of wells drilled to basement, Salinian block, central and southern Coast Ranges, California: U.S. Geological Survey Miscellaneous Field Studies Map MF-588, scale 1:500,000, 1 sheet.

Ross, D.C., 1976, Metagraywacke in the Salinian block, central Coast Ranges, California—and a possible correlative across the San Andreas fault: U.S. Geological Survey Journal of Research, v. 4, p. 683–696.

Ross, D.C., 1984, Possible correlations of basement rocks across the San Andreas, San Gregorio-Hosgri, and Rinconada-Reliz-King City faults, California: U.S. Geological Survey Professional Paper 1317, 37 p.

Ross, D.C., 1989, The metamorphic and plutonic rocks of the southernmost Sierra Nevada, California, and their tectonic framework: U.S. Geological Survey Professional Paper 1381, 159 p.

Ross, D.C., and Brabb, E.E., 1973, Petrography and structural relations of granitic basement rocks in the Monterey Bay area, California: U.S. Geological Survey Journal of Research, v. 1, p. 273–282.

Rubatto, D., 2002, Zircon trace element geochemistry, partitioning with garnet and the link between U-Pb ages and metamorphism: Chemical Geology, v. 184, p. 123–138.

Saleeby, J.B., 1997, What happens to the California Great Valley province (GVP) at its northern and southern ends?: Geological Society of America Abstracts with Programs, v. 29, no. 5, p. 62.

Saleeby, J.B., Sams, D.B., and Kistler, R.W., 1987, U/Pb zircon, strontium, and oxygen isotopic and geochronological study of the southernmost Sierra Nevada batholith, California: Journal of Geophysical Research, v. 92, p. 10443–10466.

Sherrod, D.R., and Hughes, K.M., 1993, Tertiary stratigraphy of the southern Trigo Mountains, Ariz., and eastern Chocolate Mountains, Calif.: Picacho State Park area, *in* Sherrod, D.R., and Nielsen, J.E., eds., Tertiary stratigraphy of highly extended terranes, California, Arizona, and Nevada: U.S. Geological Survey Bulletin 2053, p. 189–191.

Silver, L.T., and Anderson, T.H., 1974, Possible left-lateral Early to Middle Mesozoic disruption of the southwestern North American craton margin: Geological Society of America Abstracts with Programs, v. 6, p. 955–956.

Silver, L.T., and Nourse, J.A., 1986, The Rand Mountains "thrust" complex in comparison with the Vincent thrust-Pelona Schist relationship, southern California: Geological Society of America Abstracts with Programs, v. 18, no. 2, p. 185.

Silver, L.T., Sams, D.B., Bursik, M.I., Graymer, R.W., Nourse, J.A., Richards, M.A., and Salyards, S.L., 1984, Some observations on the tectonic history of the Rand Mountains, Mojave Desert, California: Geological Society of America Abstracts with Programs, v. 16, no. 5, p. 333.

Simpson, C., 1990, Microstructural evidence for northeastward movement on the Chocolate Mountains fault zone, southeastern California: Journal of Geophysical Research, v. 95, p. 529–537.

Sinha, A.K., Wayne, D.M., and Hewitt, D.A., 1992, The hydrothermal stability of zircon: Preliminary experimental and isotopic studies: Geochimica Cosmochimica Acta, v. 56, p. 3551–3560.

Smalley, R.F., and Isacks, B.L., 1987, A high-resolution local network study of the Nazca plate Wadati-Benioff zone under western Argentina: Journal of Geophysical Research, v. 92, p. 13,903–13,912.

Steiger, R.H., and Jäger, E., 1977, Subcommission on geochronology: Convention on the use of decay constants in geo- and cosmochronology: Earth and Planetary Science Letters, v. 36, p. 359–362.

Stern, T.W., Bateman, P.C., Morgan, B.A., Newell, M.F., and Peck, D.L., 1981, Isotopic U-Pb ages of zircon from the granitoids of the central Sierra Nevada, California: U.S. Geological Survey Professional Paper 1185, 17 p.

Tosdal, R.M., 1984, Pelona-Orocopia schist protolith: Accumulation in a Middle Jurassic intra-arc basin: Geological Society of America Abstracts with Programs, v. 16, no. 5, p. 338.

Tosdal, R.M., 1990, Tectonics of the Mule Mountains thrust system southeast California and southwest Arizona: Journal of Geophysical Research, v. 95, p. 20035–20048.

Tosdal, R.M., Haxel, G.B., and Wright, J.E., 1989, Jurassic geology of the Sonoran Desert region, southern Arizona, southeastern California, and northernmost Sonora: Construction of a continental-margin magmatic arc, *in* Jenney, J.P., and Reynolds, S.J., eds., Geologic evolution of Arizona: Arizona Geological Society Digest, v. 17, p. 397–434.

Uselding, J.E., Jacobson, C.E., and Haxel, G.B., 2001, Tertiary structural development of Orocopia Schist and related lithologies in the Peter Kane Mountain area of SE California: Geological Society of America Abstracts with Programs, v. 33, no. 6, p. 74.

Vedder, J.G., Howell, D.G., and McLean, H., 1983, Stratigraphy, sedimentation, and tectonic accretion of exotic terranes, southern Coast Ranges, California, *in* Watkins, J.S., and Drake, C.L., eds., Studies in continental margin geology: American Association of Petroleum Geologists Memoir 34, p. 471–496.

Vucic, A., Grove, M., Jacobson, C.E., and Pedrick, J.N., 2002, Multi-stage exhumation history of the Orocopia Schist in the Orocopia Mountains of southeast California: Geological Society of America Abstracts with Programs, v. 34, no. 6, p. 83.

Wood, D.J., and Saleeby, J.B., 1997, Late Cretaceous-Paleocene extensional collapse and disaggregation of the southernmost Sierra Nevada batholith: International Geology Review, v. 39, p. 973–1009.

Woodford, A.O., 1960, Bedrock patterns and strike-slip faulting in southwestern California: American Journal of Science, v. 258-A, p. 400–417.

Yeats, R.S., 1968, Southern California structure, seafloor spreading, and history of the Pacific Basin: Geological Society of America Bulletin, v. 79, p. 1693–1702.

Yin, A., 2002, Passive-roof thrust model for the emplacement of the Pelona-Orocopia schist in southern California, United States: Geology, v. 30, p. 183–186.

Yin, A., Harrison, T.M., Ryerson, F.J., Chen, W., Kidd, W.S.F., and Copeland, P., 1994, Tertiary structural evolution of the Gangdese thrust system, southeastern Tibet: Journal of Geophysical Research, v. 99, p. 18,175–18,201.